

**Correlation analysis of
subcellular ATP dynamics and
changes in cellular morphology**

February 2018

Rika Suzuki

A Thesis for the Degree of Ph.D. in Science

**Correlation analysis of
subcellular ATP dynamics and
changes in cellular morphology**

February 2018

Graduate School of Science and Technology
Keio University

Rika Suzuki

Contents

1. Chapter 1: Introduction	1
1.1 Background of this study	1
Significance of focusing on cellular morphological change	1
Relevance of ATP to cellular morphological change	1
Unsolved problem: physiological and local ATP behavior	2
Reasons for lack of studies on physiological and local ATP behavior	3
Innovation of a genetic ATP sensor for physiological and local ATP behavior	3
Additional work needed to investigate physiological and local ATP behavior	4
1.2 Purpose of this study	6
2. Chapter 2: Correlation analysis between local ATP dynamics and cellular morphological change	7
2.1 Introduction	7
2.2 Results	9
Inhibition of cytoskeletal dynamics increases local ATP	9
Cell edge has two marginal structures	13
Cell shape change by microtubule accompanying ATP increase	15
Cytoskeletons participate in change in morphology and ATP	19
2.3 Discussion	22
2.4 Materials and Methods	24
Materials	24
Plasmid construction.....	24
Cell culture.....	24
Transient transfection.....	24
Fluorescence microscopy.....	24
Image processing and analysis.....	26
Statistical Analysis.....	31
3. Chapter 3: Correlation analysis between membrane potential and ATP of mitochondria and axonal elongation	32
3.1 Introduction	32
3.2 Results	35
IMP _{mito} and ATP _{mito} in transport	35

IMP _{mito} and ATP _{mito} in fission/fusion.....	40
IMP _{mito} and ATP _{mito} in distribution.....	42
ATP _{mito} in GCs and axonal elongation have a positive correlation.....	42
ATP _{mito} in GCs are involved in axonal elongation and GC morphological change.....	45
Actin turnover is one processes related to neuronal ATP dynamics.....	51
Correlation between ATP _{mito} and IMP _{mito}	52
3.3 Discussion	55
3.4 Materials and Methods.....	59
Experimental design.....	59
Plasmid.....	59
Cell culture.....	59
Measurement of ATP _{mito} using mitAT1.03.....	60
Measurement of IMP _{mito} using TMRE.....	60
Fluorescence microscopy.....	61
Image processing and analysis of mitochondrial behavior	64
Unmixing processing	67
Image processing and analysis of neuronal behavior.....	67
Distinguishing transport categories.....	68
Analysis of fusion and fission events.....	68
Visualizing the correlation between ATP _{mito} levels and IMP _{mito}	69
Correlation analysis and random shuffling	69
Comparison of mitochondrial properties in the GC and axonal process.....	69
Inhibitor experiments	69
Quantification of morphological change in growth cone.....	70
Imaging of cytosolic ATP level	70
Statistical analysis.....	70
4. Chapter 4: Conclusion	71
4.1 Summary.....	71
4.2 Significance.....	75
4.3 Features and advantages of this approach	77
Analysis without artificial intervention.....	77
Analysis without extreme conditions.....	77
Analysis without prior identification of analytical targets	77
4.4 Potential applications of this approach.....	78

Combination with signal transduction analysis.....	78
Combination with system perturbation	78
References.....	79
List of published papers and conference presentations	
Acknowledgment	

1. Chapter 1

Introduction

1.1 Background of this study

Significance of focusing on cellular morphological change

Each cell has its own morphology, which is thought to be related to its function (Lamprecht and LeDoux, 2004; Yuste and Bonhoeffer, 2001), therefore, appropriate morphology is crucial for cells. Since morphology and function are closely related, irregular morphological dynamics are thought to be harmful for proper cellular function. In fact, some neurodegenerative diseases have been shown to accompany damaged cellular morphology (Dubey et al., 2015; Plucińska et al., 2012; Takihara et al., 2015; Wang et al., 2016).

Relevance of ATP to cellular morphological change

Adenosine triphosphate (ATP) is one factor that may be related to morphological dynamics (Bernstein and Bamberg, 2003; Fukumitsu et al., 2015; Oruganty-Das et al., 2012; Rangaraju et al., 2014; Spillane et al., 2013). In special neurons, the Purkinje cells, inhibition of mitochondrial delivery results in low ATP levels at the edges of dendrites, as well as in reduced actin dynamics (Fukumitsu et al., 2015). Hippocampal neurons lacking cytoplasmic polyadenylation element binding protein 1 (CPEB1) exhibit mitochondrial dysfunction and reduced ATP levels, resulting in defective dendrite morphogenesis (Oruganty-Das et al., 2012). As with other ATP-related morphological changes in the neuronal spines, neuronal activity is known to enhance ATP consumption (Attwell and Laughlin, 2001; Harris et al., 2012; Rangaraju et al., 2014). Recycling of synaptic vesicles requires a large amount of ATP, which may be because of the dynamin that mediates membrane fission (Rangaraju et al., 2014). These local morphological changes have also been reported in other cell types. In tumor cells, increased cell motility and invasion induced by phosphatidylinositol 3-kinase (PI3K)

activity accompanies redistribution of their mitochondria to the cortical cytoskeleton (Caino et al., 2015). In endothelial cells, the lamellipodia (structures localized in leading-membrane ruffles and rich in actin) contain several small regions in which ATP levels are relatively high (De Bock et al., 2013).

Unsolved problem: physiological and local ATP behavior

However, these previous findings are mainly based on perturbations of energy metabolism, and ATP dynamics and their relevance to morphological change under physiological conditions are still poorly understood. Although some studies have monitored intracellular ATP levels, they mostly measured changes in response to strong stimuli that induced extensive intracellular changes in ATP levels (Fukumitsu et al., 2015; Oruganty-Das et al., 2012; Rangaraju et al., 2014). Cellular ATP dynamics under normal **physiological conditions** are thus not yet well understood.

In addition, there is a lack of research focused on **local** ATP dynamics. Some cellular biophysical and/or biochemical processes, such as the synthesis of new proteins, the reorganization of cytoskeletons, and the functioning of ATP/GTPase, require ATP during cellular morphological change (Ataullakhanov and Vitvitsky, 2002; Hara and Kondo, 2015; Rolfe and Brown, 1997). However, previous findings suggest that the one that requires the most ATP is actin turnover. One estimate suggested that this process is responsible for 50% of the ATP turnover in platelets (Daniel et al., 1986). Since actin localizes heterogeneously within a cell, fluctuation in ATP levels related to actin dynamics may also not be uniform throughout the cell. Furthermore, in general, activeness of cellular morphological change are also not uniform within a cell; in most cases, the peripheral areas of the cell show higher activity than the areas near the center of the cell body (Caino et al., 2015; De Bock et al., 2013). Therefore, local ATP levels should be considered when investigating the relationship between ATP and morphological change. However, most previous studies have estimated ATP levels as average values for whole cells (Connolly et al., 2014; Dalton et al., 2014; Surin et al.,

2012; Tanaka et al., 2014), and the intracellular varieties of distribution and dynamics of ATP are as yet unknown.

Reasons for lack of studies on physiological and local ATP behavior

It is likely that one of the reasons for this lack of research into *physiological and local ATP behavior* is that it is not possible to perform sufficiently high-resolution spatiotemporal quantification under physiological conditions using conventional ATP-measuring methods. One of the conventional methods, ^{31}P nuclear magnetic resonance (NMR), requires cellular lysate, i.e., cellular spatial information is lost. Monitoring temporal changes within a cell is also impossible using this method (McLaughlin et al., 1979). Another conventional approach, the luciferase assay, requires a large excess quantity of the enzyme to quantitatively measure the change in ATP levels (Strehler and McElroy, 1957); it does not therefore reflect normal physiological conditions.

Innovation of a genetic ATP sensor for physiological and local ATP behavior

In this context, a novel genetic ATP sensor (Imamura et al., 2009) has been developed to overcome these problems. This is a fluorescence resonance energy transfer (FRET)-based indicator, and is composed of the epsilon subunit of the F_0F_1 -ATP synthase sandwiched between cyan- and yellow-fluorescent proteins. FRET is a phenomenon that occurs between donor and acceptor molecules. When the emission spectrum of a donor overlaps the absorption spectrum of an acceptor, the energy of the excited donor is transferred to the acceptor. This occurs when the two molecules are in close proximity, although the extent of the spectral overlap between donor and acceptor, as well as their orientation, affects the efficiency of the FRET. The epsilon subunit largely changes its morphology into a folded form upon ATP binding, which is relaxed in the absence of ATP. As result, the change in ATP levels can be estimated based on the change in FRET signal (Imamura et al., 2009). Because this sensor is genetically encoded, time-lapse imaging with a high spatiotemporal resolution within living cells should be possible.

Additional work needed to investigate physiological and local ATP behavior

Nevertheless, there are only a few studies that have explored physiological or local ATP dynamics. Considering that ATP estimation using averaged whole-cell values (Connolly et al., 2014; Dalton et al., 2014; Nakano et al., 2011; Surin et al., 2012; Tanaka et al., 2014), and observation of ATP change in response to extensive stimuli (Connolly et al., 2014; Surin et al., 2012; Tanaka et al., 2014) have been conducted using the genetic ATP sensor, the remaining challenges for investigating physiological or local ATP behavior appear to be related to developing appropriate analyses. For instance, since cell morphology changes dynamically at cell edges, quantifying local ATP dynamics in such areas requires image-processing analysis that is able to track changes in cellular morphology. Moreover, in general, change in ATP levels without extensive stimulation is subtle; therefore, a suitably sensitive procedure is needed to evaluate this change.

However, recently, several bio-imaging studies have succeeded in demonstrating relationships among biological signals collected from simultaneous fluorescence imaging under physiological conditions (Kobayashi et al., 2013; Tsukada et al., 2008; Zawistowski et al., 2013). Common to all of them is a combination of spatiotemporal image processing and cross-correlation analysis. Tsukada et al. conducted a correlation analysis between Ras-related C3 botulinum toxin substrate 1 (Rac1) activity and cellular morphological change and found a positive correlation (Fig. 1-1) (Tsukada et al., 2008). Zawistowski et al. reported a correlation-analysis between the protrusion velocity of the cell edge and either Ras homolog family member A (RhoA) or Ras homolog family member C (RhoC) activity (Zawistowski et al., 2013). They showed that RhoA and RhoC are differentially regulated in cell protrusions, with distinct kinetics in several areas, which are defined by their distance from the cell edge (Fig. 1-2). Both studies involved extensive image-processing analysis after simultaneous fluorescence imaging, followed by an evaluation of the signals using cross correlation analysis. This approach facilitates local quantification and exploratory correlation analysis, and also appears to be useful for the study of *physiological and local ATP behavior*.

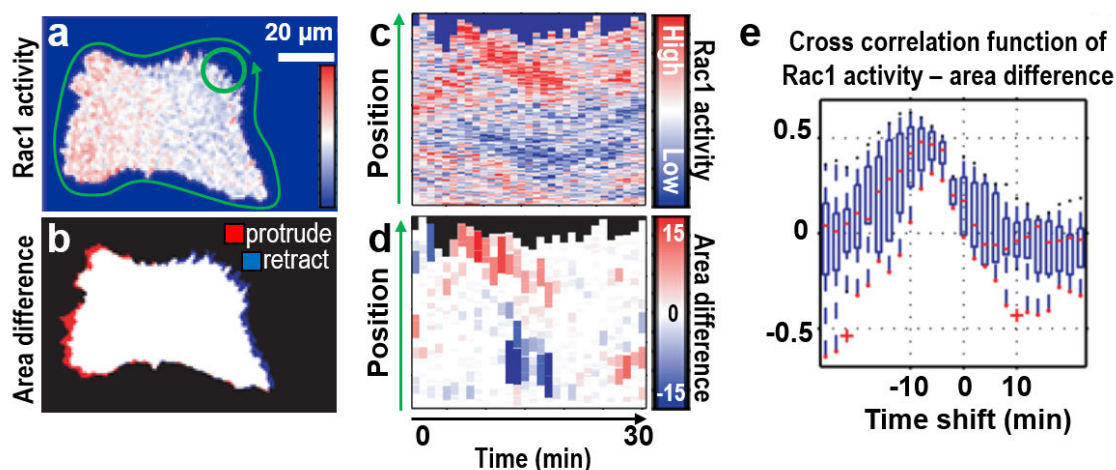


Figure 1-1. Cross correlation analysis between Rac1 activity and change in cellular area.

(a, b) Pseudo-color visualization of (a) Rac1 activity and (b) change in cellular area. (c, d) Corresponding heat maps for (c) panel a and (d) panel b. (e) Cross correlation between Rac1 activity and change in area. Source: © 2008 Tsukada et al., adapted.

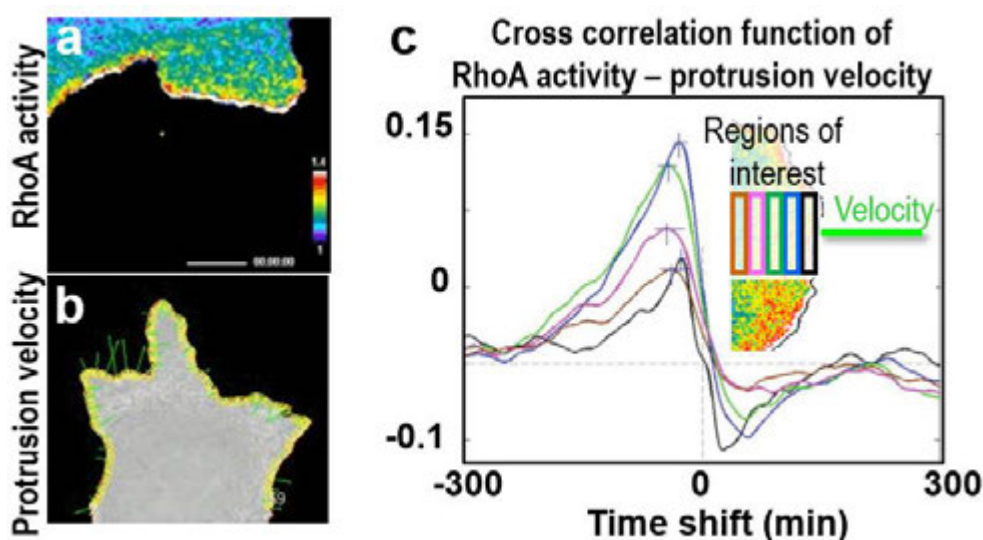


Figure 1-2. Cross correlation analysis between RhoA activity and protrusion velocity.

(a) Pseudo-color visualization of RhoA activity. (b) Protrusion velocities of cell edges represented by green lines. (c) Cross correlation between RhoA activity and protrusion velocity. Black: 0–0.9 μm, blue: 0.9–1.9 μm, green: 1.9–2.8 μm, pink: 2.8–3.7 μm, brown: 3.7–4.6 μm from the cell edge. A similar analysis was also conducted for RhoC. Source: © 2013 Zawistowski et al., adapted.

1.2 Purpose of this study

As mentioned above, although local cellular ATP dynamics seem to be important and related to local morphological changes, no studies have yet demonstrated this under physiological conditions. However, I hypothesized that this could be done by combining the genetic ATP sensor with image processing and correlation analysis. In this context, the purpose of this study is to visualize physiological ATP dynamics and to explore how these relate to cellular morphological change in HeLa cells (Chapter 2) and in neurons (Chapter 3), using ATP imaging, image processing, and correlation analysis (Fig. 1-3).

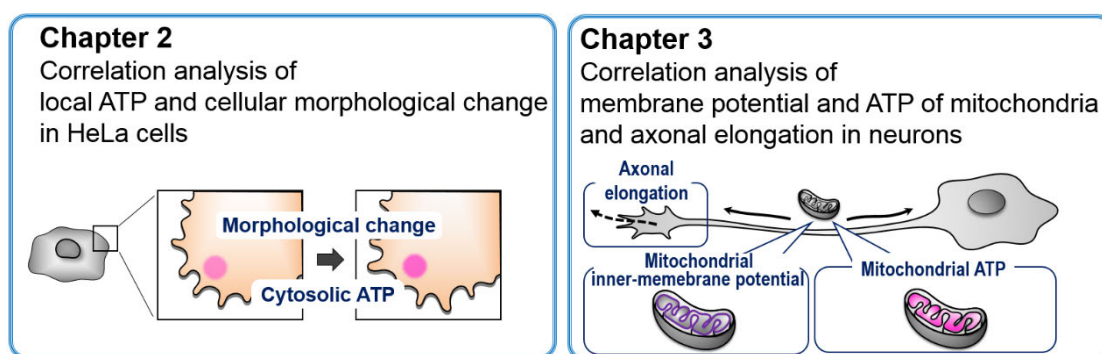


Figure 1-3. Overview of this study.

(left) Chapter 2 reports on a cross correlation analysis between cytosolic ATP dynamics and cellular morphological change in HeLa cells. (right) Chapter 3 reports on a cross correlation analysis between mitochondrial activity (inner-membrane potential and ATP levels in the mitochondrial matrix) and axonal elongation in neurons.

2. Chapter 2

Correlation analysis between local ATP dynamics and cellular morphological change

2.1 Introduction

Adenosine triphosphate (ATP) is a major energy source for cells, and is used in muscle contraction (Cain and Davies, 1962), neuronal activity (Harris et al., 2012), organ development (Massé et al., 2007), and many other physiological phenomena.

Investigations into intracellular ATP levels have been limited, mostly centered on how they change in responses to 2-deoxyglucose (2-DG) or glucose, which perturb energy metabolism (Ainscow and Rutter, 2002; Surin et al., 2012; Tanaka et al., 2014), and during hypoxia or excitotoxicity (Connolly et al., 2014; Kioka et al., 2014; Toloe et al., 2014). The nature of ATP fluctuation in living cells under normal and physiological conditions is still largely unknown.

ATP-related cellular and subcellular phenomena include cytoskeletal dynamics (Bernstein and Bamburg, 2003) and cellular morphological changes (De Bock et al., 2013; Oruganty-Das et al., 2012; Rangaraju et al., 2014). In chick ciliary neurons, ATP depletion suppresses actin turn-over and long-term ATP depletion causes changes in cellular shape (Bernstein and Bamburg, 2003). Hippocampal neurons lacking cytoplasmic polyadenylation element binding protein 1 (CPEB1) have brain-specific dysfunctional mitochondria and reduced ATP levels, which result in defective dendrite morphogenesis (Oruganty-Das et al., 2012). Also, in neuronal spines, neuronal activity increases ATP consumption. Synaptic vesicle recycling presents a large ATP burden, which may be because of dynamin that mediates membrane fission (Rangaraju et al., 2014). These previous reports indicate that variation in ATP levels is related to cellular morphological changes and cytoskeletal dynamics.

To demonstrate the presence of a direct relationship under physiological conditions, precise and simultaneous observation of ATP levels and either cellular morphology or cytoskeletal dynamics is necessary. This has been difficult because conventional ATP quantification methods do not allow for high-resolution observation (Imamura et al., 2009). Although the technical development of the novel genetic ATP sensor ATeam enabled such observations (Imamura et al., 2009), finding the relationships is still not easy, because, in general, fluctuation in biological signals without extensive stimulation is subtle and occurs over a narrow range. Despite this technical challenge, we recently successfully investigated the relationship between the motility of the growth cone and the crosstalk of second messengers through a combination of simultaneous imaging with spatiotemporal image processing analysis (Kobayashi et al., 2013).

In this study, we combined simultaneous imaging with detailed analysis to reveal the relationships between cytoskeletal dynamics, morphological change, and ATP level change. We conducted several kinds of simultaneous imaging using ATeam, an indicator for microtubule dynamics that used fluorescent-labeled EB3 (end-binding protein 3) (Matov et al., 2010; Morrison et al., 2002; Stepanova et al., 2003), fluorescent-labeled actin, and fluorescent dye for the plasma membrane (FM4-64) in HeLa cells. We quantified the spatiotemporal behavior of the cells using our original image processing software, and revealed that cytoskeletal dynamics at the cell edge are related to cellular morphology and intracellular ATP levels, and that actin and microtubules influence them in different ways.

2.2 Results

Inhibition of cytoskeletal dynamics increases local ATP

Our goal was to reveal the relationships between change in intracellular ATP levels, cytoskeletal dynamics, and morphological change in HeLa cells under physiological conditions. To verify whether these relationships exist, we first examined if the inhibition of cytoskeletal dynamics affect intracellular ATP levels. HeLa cells expressing ATeam were imaged under physiological conditions for 10 min, and cytoskeletal dynamics were modulated by 100 nM Latrunculin A or 200 nM Taxol at 3 min. Latrunculin A binds with 1:1 stoichiometry to monomeric actin (Spector et al., 1999), sequesters monomers, and prevents their reassembly (Morton et al., 2000). Latrunculin A-treated cells are known to lose their focal adhesions and retract (Wang et al., 2005). Taxol specifically binds to and stabilizes microtubules (Downing, 2000). Application of Taxol completely abolishes the binding of microtubule-associated proteins to the ends of growing microtubules (Stepanova et al., 2003), therefore disrupting microtubule dynamics (Matov et al., 2010). As expected, Latrunculin A caused retraction in 8/8 cells (Fig. 2-1a). 6/7 Taxol-treated cells also showed morphological change (Fig. 2-1d). Because the degree of retraction differed by location, we separated each cell into 8 compartments (Fig. 2-1a, d), and quantified spatiotemporal ATP levels and cellular morphology within each compartment (Fig. 2-1b, e). Statistical analysis revealed that cells treated with Latrunculin A showed ATP levels that were increased only at the edge part, while Taxol-treated cells exhibited increased ATP levels at both the central and the edge parts (Fig. 2-1c, f). On the other hand, 10 mM 2-DG (in 3/3 cells) and 1 μ M FCCP (carbonyl cyanide-p-trifluoromethoxyphenylhydrazone, in 3/3 cells), which suppress ATP production, lowered relative ATP levels throughout the cell without any place dependency (Fig. 2-2). FCCP is a protonophore, which is known to cause calcium leak from mitochondria, so the leaked calcium might have influences on the cytoskeleton or ATP levels. We also confirmed that FCCP increased calcium levels (Fig. 2-2g), although neither FCCP nor ionomycin, which causes a larger calcium leak than FCCP, induced significant changes in morphology in the cellular areas examined (Fig. 2-2g, h). From the above, the results suggest cytoskeletal dynamics are related to change in ATP levels, especially at the cell edge. Moreover, the influence

upon cellular morphology and ATP levels differs depending on whether actin or microtubule dynamics are involved.

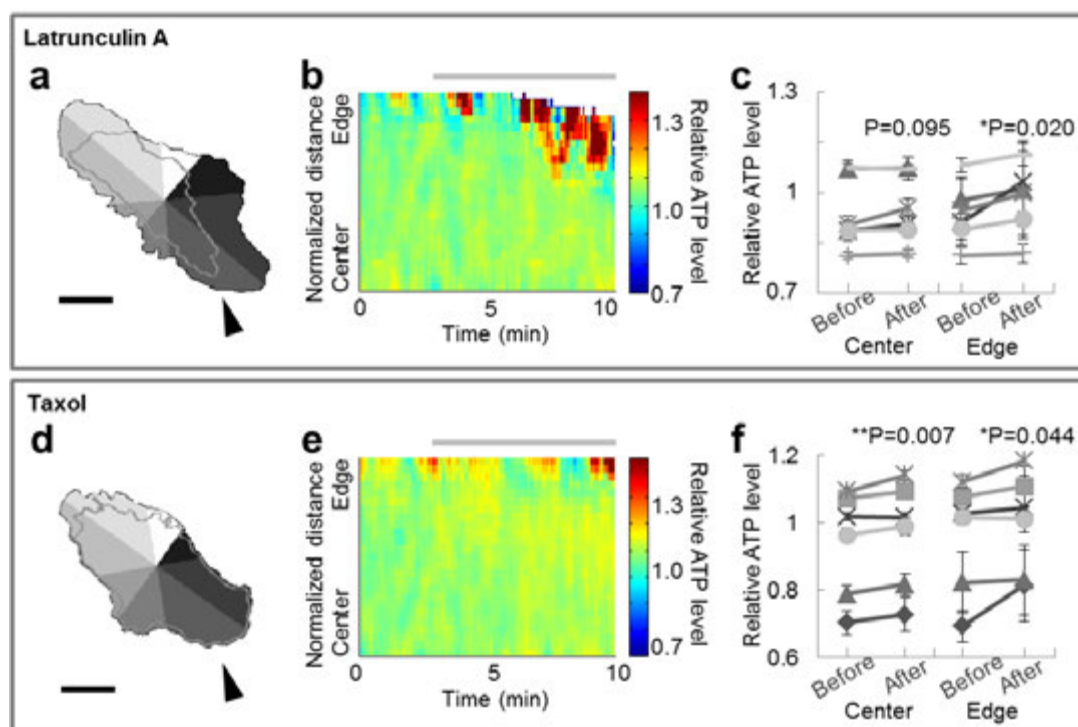


Figure 2-1. Inhibition of cytoskeletal dynamics induces an increase in local ATP.

(a, d) Typical images of the cellular morphology at the beginning of the observation. The gray-shaded regions represent 8 automatically divided compartments, while the gray line depicts the cellular morphology at the end of the observation. Scale bar represents 30 μm . (b, e) Typical image of the spatiotemporal behavior of intracellular relative ATP levels in the compartment indicated by the arrowhead in the left figure. The horizontal axis indicates time, the vertical axis indicates position, and pseudo color indicates relative ATP level. Each color lookup table is linear and covers the full range of the data. The gray bar indicates the duration of inhibition. (c, f) Comparisons of relative ATP level before and after inhibition at the central and edge parts. When cells were treated with Latrunculin A, relative ATP level increased only at the edge ($n = 6$). On the other hand, Taxol-treated cells showed an increase in relative ATP level at both the central and the edge parts ($n = 6$). Error bar represents standard deviation (SD).

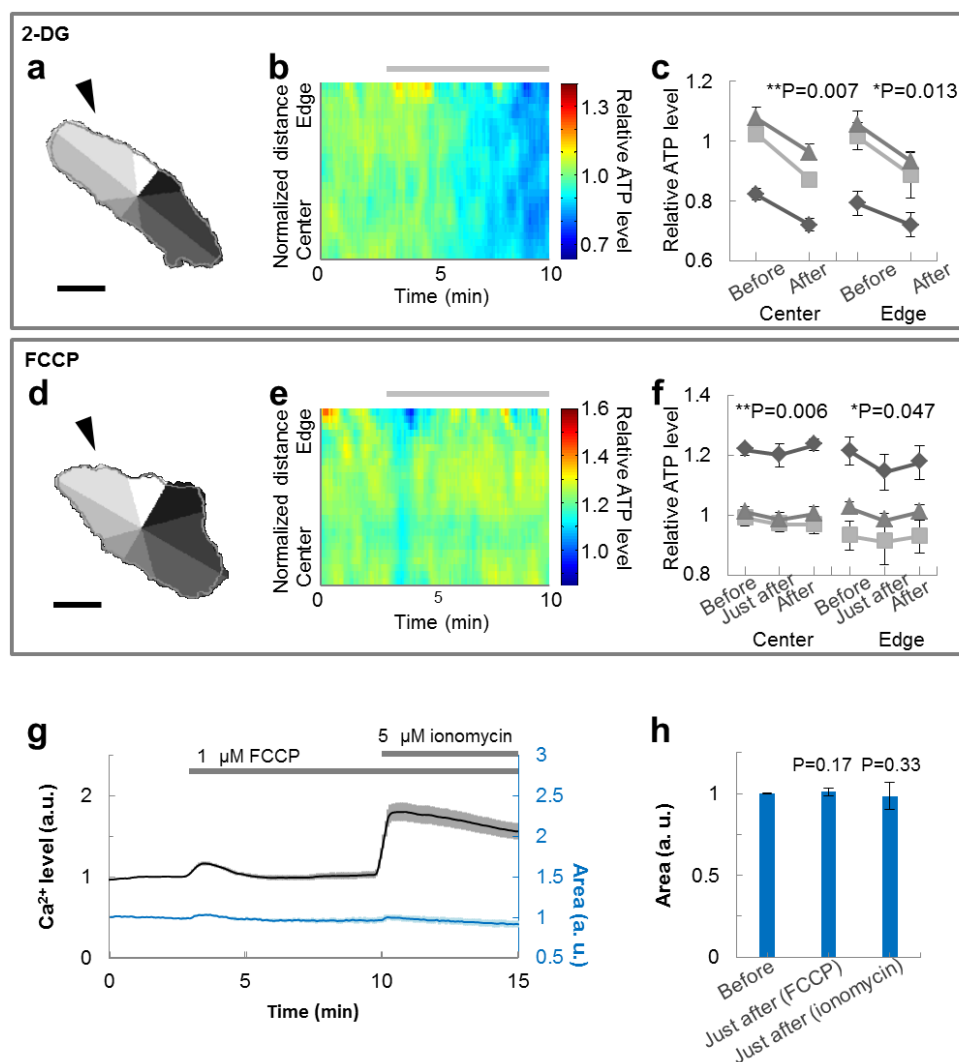


Figure 2-2. Reduction of ATP levels throughout the cell from the inhibition of ATP synthesis.

(a, d) Typical images of the cellular morphology at the beginning of the observation. The gray-shaded regions represent 8 automatically divided compartments, while the gray line depicts the cellular morphology at the end of the observation. Scale bar represents 30 μm . (b, e) Typical images of the spatiotemporal behavior of intracellular relative ATP levels in the compartment indicated by the arrowhead in the left figure. The horizontal axis indicates time, the vertical axis indicates position, and the pseudo color indicates the ATP level. Each color lookup table is linear and covers the full range of the data. The gray bar indicates the duration of inhibition. (c, f) Comparisons of ATP levels before and after the inhibition at the central and edge parts. When cells were treated with glycolysis inhibitor 2-DG, ATP levels decreased throughout the cell ($n = 3$). Mitochondria uncoupler carbonyl cyanide-p-trifluoromethoxyphenylhydrazone (FCCP)-treated cells showed reduced ATP levels just after inhibition but then recovered; the decrease occurred throughout the cell ($n = 3$). Error bar represents SD.

(g) Changes in cytosolic calcium levels (black, left axis) and cell area (blue, right axis). Cells were loaded with Fluo-4 AM by incubation with 10 μM Fluo-4 AM with 0.02 w/v% F-127 for 30 min followed by a 15 min de-esterification period. FCCP (final 1 μM) was applied at 3 min and ionomycin (final 5 μM) was added at 10 min during the 15 min imaging. FCCP caused a slight transient increase in calcium levels (30 cells from 5 dishes). Error bar represents standard error of the mean (SEM). (h) Statistical evaluation of changes in cell area. Application of neither FCCP nor ionomycin induced a significant change in cell area (30 cells from 5 dishes). Error bar represents SEM.

Cell edge has two marginal structures

Cytoskeletal-dynamics-related changes in morphology and intracellular ATP levels were remarkable at the cell edge. We therefore focused the next stages of our research on the cell edge. We considered it necessary to visualize actin and microtubule separately because their influence upon ATP levels and cell morphology were different. We first observed HeLa cells expressing EB3-Venus. EB3 is a protein which binds to the plus end of a microtubule during elongation growth, and fluorescent-labeled EB3 acts as an indicator for microtubule dynamics (Matov et al., 2010; Morrison et al., 2002; Stepanova et al., 2003). EB3-Venus was found not only at the plus ends of microtubules, but also diffused throughout the cytosol (Fig. 2-3a). However, the fluorescent dye for the lipid bilayer, FM4-64, revealed that there is also the peripheral structure consisted of actin, which was not visualized by EB3-Venus (Fig. 2-3a, b). The region EB3-Venus diffused into is called the ‘lamella’ and the peripheral structures outside the lamella are called ‘filopodia’ or ‘lamellipodia’ (Ladoux and Nicolas, 2012; Machacek and Danuser, 2006). Up to here, we have conceptually grouped these regions by the term ‘edge’, but we will now begin to consider them separately, calling them ‘lamella’ and ‘peripheral structure’, respectively.

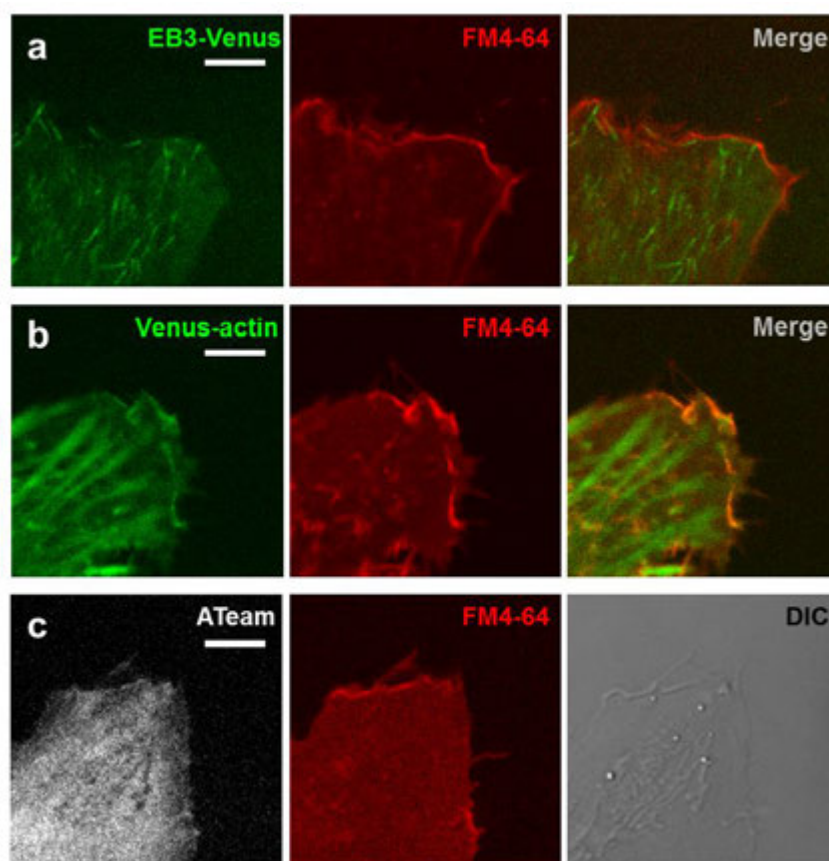


Figure 2-3. Structure at the cell edge: the lamella and the peripheral structure are distinguished.

(a) Typical EB3-Venus (left), FM4-64 (middle), and merged (right) images at the edge of a HeLa cell. EB3 probe diffused throughout the cytosol. (b) Typical Venus-actin (left), FM4-64 (middle), and merged (right) images at the edge of a HeLa cell. The peripheral structure of the cell edge is constructed of actin filaments. (c) Typical images of (msecCFP+mVenus) fluoresce of ATeam (left), FM4-64 (middle), and differential interference contrast (DIC; right) at the edge of a HeLa cell. The peripheral structure at the cell edge was detectable from the (msecCFP+mVenus) signal. Scale bar represents 5 μm .

Cell shape change by microtubule accompanying ATP increase

We explored whether these two layers were related through simultaneous observation of EB3-labeled microtubules and the peripheral structure visualized by FM4-64. These observations revealed that the peripheral structure showed high motility where the dynamics of EB3-labeled microtubule were active. This peripheral movement was suppressed by Taxol-induced inhibition of microtubule dynamics. As mentioned in many previous reports, disturbance of microtubule dynamics negatively affects actin dynamics and cellular morphology, which could be rescued by actin stabilization (Jaworski et al., 2009; Swiech et al., 2011), suggesting that microtubule dynamics are upstream of actin dynamics. Indeed, we found no obvious effects on microtubule dynamics in Latrunculin-A treated cells (Fig. 2-4). So, we focused on microtubule dynamics first, examining the relationships between microtubule dynamics and change in cellular morphology or ATP levels. In EB3-mCherry expressing cells under physiological conditions, microtubules rushed into and touched the lamella boundary, changing the lamella shape (Fig. 2-5). Next, we observed HeLa cells co-expressing EB3-mCherry and ATeam to explore how these microtubule dynamics affect intracellular ATP levels. We chose the region of interest (ROI) at the cell edge, and acquired time-series data of EB3 density, the number of newly generated lamella areas, and relative ATP levels (Fig. 2-6a). We constructed a cross correlation function between newly generated lamella areas and EB3 density (Fig. 2-6b). Since a negative peak at 0 min is a result of parameter properties (as EB3 density is defined as the value of (EB3 positive pixel) / (cell area positive pixel), it decreases when the newly generated lamella area increases), we focused only on the positive peaks. There were three positive peaks at -7 min, -2.5 min and 3 min, suggesting that cross correlation analysis would be required within 5 min. Then, we averaged the waveforms in the duration between before and after two minutes the timing of a peak in the number of newly generated lamella areas. This analysis showed that EB3 density increases about 1 min before the peak in newly generated lamella areas and that this area growth accompanies an increase in the relative ATP level (Fig. 2-6c, solid line). This increase was not obvious in the calculations using randomly shuffled datasets (Fig. 2-6c, broken line). Moreover, inhibition of microtubule dynamics by Taxol reduced the number of EB3 particles and

EB3 contacts with the lamella boundary, therefore suppressing cellular morphological change that was obvious under physiological conditions (Fig. 2-4). From the above findings, microtubule rush appear to increase the lamella area at the cell edge and this increase involves a rise in ATP levels.

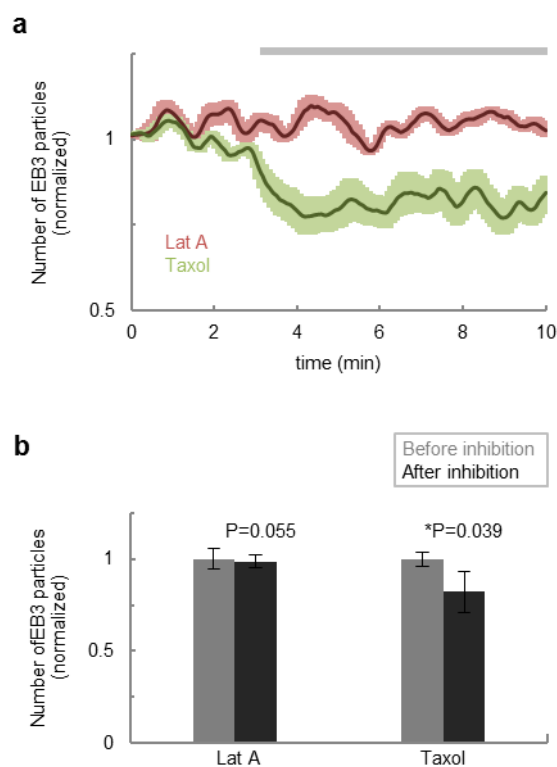


Figure 2-4. Taxol reduced the number of EB3 particles.

(a) Averaged time-course of the number of EB3 particles at the cell edge when cells were treated with Latrunculin A ($n = 5$) or Taxol ($n = 5$). The gray bar indicates the duration of inhibition. (b) Statistical analysis revealed the number of EB3 particles was reduced by Taxol, but not by Latrunculin A. Error bar represents SEM.

Correlation analysis between local ATP dynamics and cellular morphological change

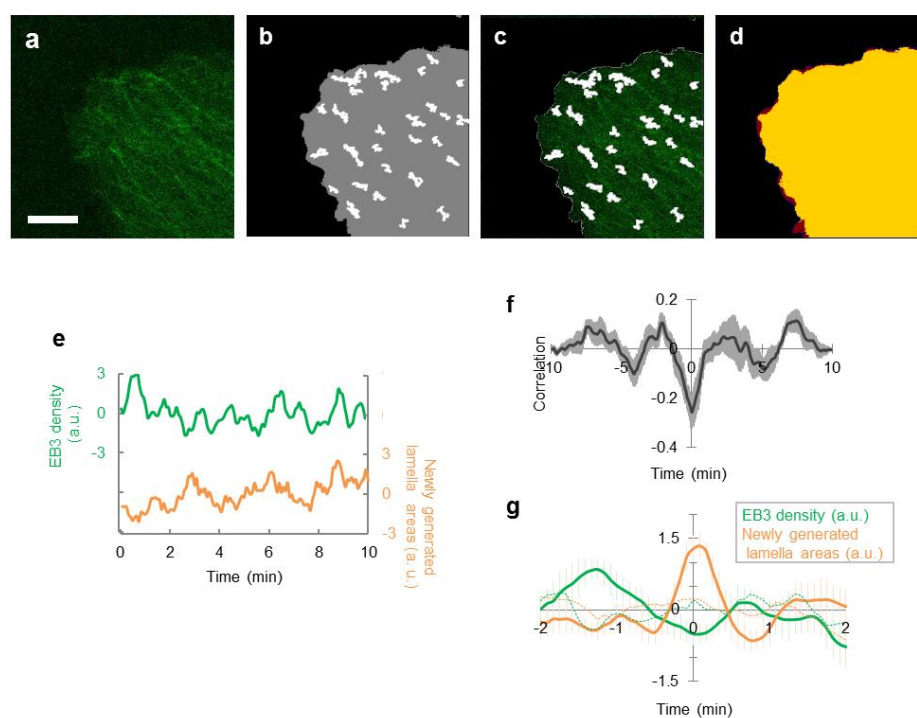


Figure 2-5. Microtubule dynamics cause HeLa cells to change shape.

(a) A typical image of the edge of a HeLa cell expressing EB3-mCherry. (b) Detected EB3 particles. Scale bar represents 5 μm . (c) Overlapped image of Fig. 2-5a and Fig. 2-5b. (d) Time-differential image of cell morphology. Red-colored pixels represent newly generated pixels. (e) Typical time courses of EB3 density (green) and the number of newly generated lamella areas (orange) within an ROI. (f) Cross correlation function between the number of newly generated lamella areas vs. EB3 density. Positive correlation was observed every 5 min (11 ROIs from 8 cells). (g) An average of waveforms in duration between before and after the timing when the number of newly generated lamella areas show peak (8 events from 8 cells). EB3 density increases about 1 to 2 min before the peak. No apparent peak was observed in the average of waveforms from randomly shuffled datasets (broken lines). Error bar represents SEM.

Correlation analysis between local ATP dynamics and cellular morphological change

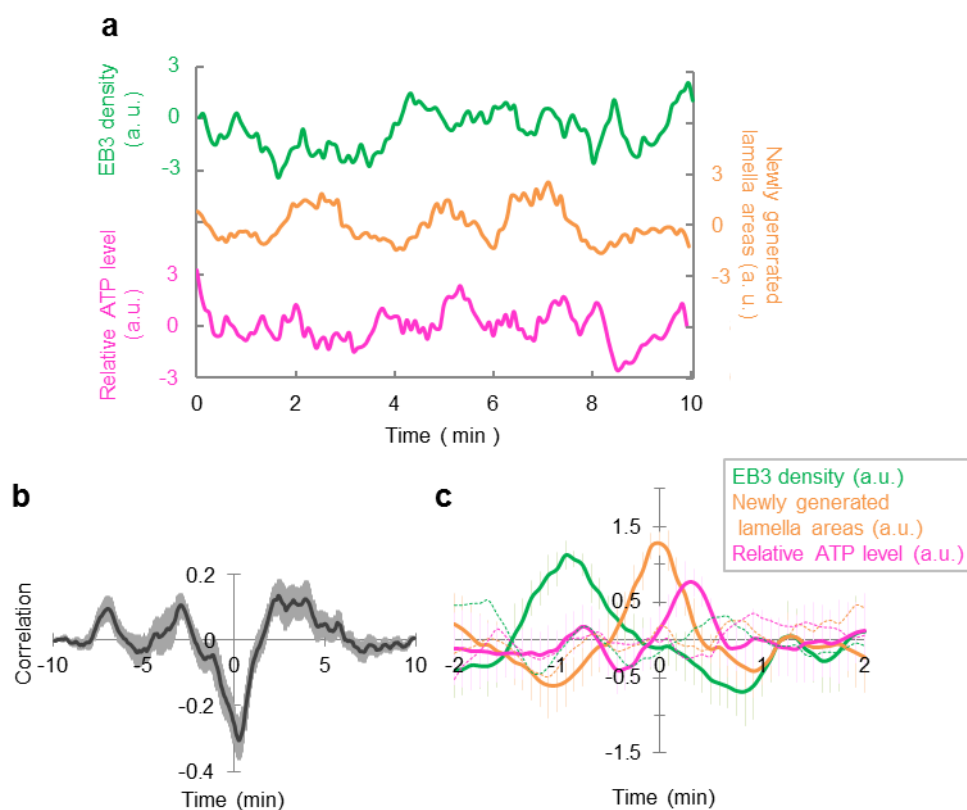


Figure 2-6. Microtubule dynamics cause a change in cell shape, which is accompanied by an increase in the ATP level at the cell edge.

(a) Typical time courses of EB3 density (green), the number of newly generated lamella areas (orange), and the relative ATP level (pink) within an ROI. (b) Cross correlation function between newly generated lamella areas vs. EB3 density. Positive correlations were observed at -7 min, -2.5 min, and 3 min (12 ROIs from 6 cells). (c) An average of waveforms in the duration between before and after the timing of a peak in the number of newly generated lamella areas (solid line, 9 ROIs from 6 cells). EB3 density increased about 1 min before the peak and this increase in the lamella area accompanied an increase in the relative ATP level. No apparent peak was observed in the average of waveforms from randomly shuffled sequences (broken lines). Error bar represents SEM.

Cytoskeletons participate in change in morphology and ATP

We revealed that microtubule dynamics are not only associated with change in morphology and ATP levels at the lamella, but to motility of peripheral structure consisting of actin. Actin requires ATP for polymerization, so we posited that ATP level changes observed in the lamella that is related to microtubule dynamics could be linked to the morphological change of the peripheral structure. We observed HeLa cells expressing ATeam with high spatial resolution, which enabled us to collect data on not only ATP levels but also the appearance of the peripheral structure (Fig. 2-3c). The lamella was assumed to correspond to the region 1–2 μm interior from the cell edge (Fig. 2-3), and exterior to this lamella region was defined as the peripheral structure. We set a small ROI at the cell edge where morphology dynamically changed, then estimated protrusion length of the peripheral region by measuring distance from the tip of the peripheral structure to the lamella. In addition, we calculated relative ATP level near the protrusion within the lamella and then plotted the time change of relative ATP level and protrusion length. The plot continuously varied within the range of ~ 0.7 relative ATP level and ~ 3 μm of protrusion length over 25 min (Fig. 2-7a, h), visualizing very intricate tracks. To investigate the origin of these complicated tracks, we applied Latrunculin A, Taxol, or 2-DG at 5 min and conducted the imaging for 15 min. Since the inhibitory effects of Latrunculin A, Taxol and 2-DG did not appear immediately after their application, and the time lags differed among cells, we analyzed the effect of the inhibitors on protrusion length and relative ATP levels in the last 5 min (pink-colored time period in Fig. 2-7a–d). We calculated the range of relative ATP levels and the protrusion length within the last 5 min as percentages of the total 15 min (Fig. 2-7e–j). In Latrunculin A-treated cells, the dynamic range of track distance was extremely narrow in the last 5 min. The tracks also converged at the point of a short protrusion length and a high relative ATP level (Fig. 2-7b, e, i, j). Time-lapse fluorescent imaging also showed that Latrunculin A treatment diminished the peripheral structural area. Therefore, Latrunculin A reduces the area of the actin-based structure, which could increase ATP levels. The dynamic range of relative ATP levels and the protrusion length of the tracks in the last 5 min decreased when cells were treated with Taxol (Fig. 2-7c, f, i, j). Time-lapse fluorescent imaging demonstrated that not only the peripheral

structure but also the lamella retracted, which is different from the morphological change caused by Latrunculin A. These observations suggest that Taxol treatment deprived cells of the changes in morphology and the ATP levels observed within the lamella, which resulted in a decrease in protrusion length. On the other hand, in cells treated with 2-DG, tracks in the last 5 min showed a drastic decrease in relative ATP levels as well as scanty cell edge motility (Fig. 2-7d, g, i, j). This suggests that ATP would be required for morphological changes. Taken together, these findings indicate that morphological change in the peripheral structure is associated with ATP level change, and while actin dynamics play a great role, microtubule dynamics are also related. We reasoned that these two kinds of influences upon ATP levels and cellular morphology could explain the complexity of the tracks. The tracks showed both right-handed and left-handed rotations and shifted between both rotations sequentially, indicating that ATP level is not always preferentially controlled over the protrusion length, nor *vice versa*. It could be reasonable to consider the complexity of the tracks is a consequence of the complex mixture of these two effects on ATP levels and protrusion length. In summary, at the cell edge, morphological change in peripheral structure and ATP levels are affected primarily by actin dynamics, but also, weakly, by microtubule dynamics.

Correlation analysis between local ATP dynamics and cellular morphological change

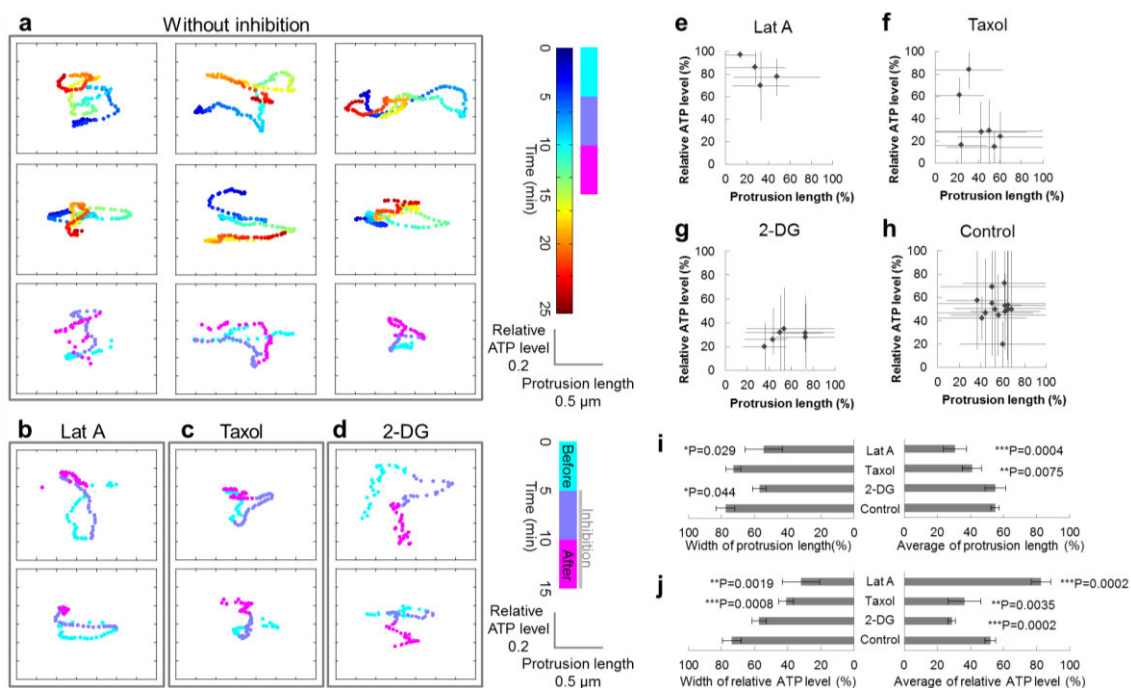


Figure 2-7. Both actin and microtubule dynamics affect cellular ATP levels at the cell edge.

(a) Typical tracks of protrusion length and ATP levels at the edges of HeLa cells under physiological conditions (9 examples from 5 cells). The horizontal axis indicates protrusion length, the vertical axis indicates relative ATP levels, and the pseudo color indicates time. (b–d) Typical tracks of HeLa cells treated with (b) Latrunculin A (left, 2 examples from 2 cells), (c) Taxol (middle, 2 examples from 2 cells), or (d) 2-DG (right, 2 examples from 2 cells). During the last 5 min of observation (pink), the tracks of Latrunculin A-treated cells lost their movement, while a reduced range of variation in relative ATP levels was observed in the tracks of Taxol-treated cells. Cells treated with 2-DG showed decreased motility as well as ATP levels. (e–h) Ranges of measured values in the last 5 min as percentages of the total timeframe. Markers indicate the mean values, while bars indicate the ranges. (i, j) Statistical analysis of (left) width and (right) average values of the ranges of (i) protrusion length and (j) relative ATP levels (4 ROIs from 2 cells for Latrunculin A, 7 ROIs from 3 cells for Taxol, 6 ROIs from 2 cells for 2-DG, and 15 ROIs from 6 cells for control).

2.3 Discussion

We conducted various simultaneous imaging and spatiotemporal analyses of intracellular ATP levels, cytoskeletal dynamics, and cellular morphological change, and revealed striking correlations among them.

Actin dynamics are reportedly related to ATP levels (Bernstein and Bamburg, 2003) and we confirmed this assertion through experiments with Latrunculin A (Fig. 2-1a–c and Fig. 2-7b, e, i, j). Our results indicated that intracellular ATP level at the cell edge is influenced by not only actin dynamics but also microtubule dynamics. Although the effect of microtubule dynamics seemed less distinct than that of actin (Fig. 2-7b, c, e, f, i, j), a combination of simultaneous imaging and image processing analyses enabled us to demonstrate its presence.

Cultured hippocampal neurons derived from CPEB1 knock out (KO) mice showed a decrease in ATP production and fewer dendrite branches (Oruganty-Das et al., 2012). When these CPEB1 KO neurons were cultured in medium containing phosphocreatine for 4 days *in vitro*, ATP levels recovered to nearly wild type levels, as did dendritic branches. Although these results suggest ATP is important for neurite outgrowth and morphogenesis, the relevance between them were not asserted. This is because intracellular ATP levels and cell morphology were observed in different cells: that is, not coincidentally. Our simultaneous imaging conducted here succeeded in directly showing that cytoskeletal dynamics induce changes in intracellular ATP levels and cellular morphology.

Several cellular mechanisms can produce spatiotemporal heterogeneity in ATP distribution. The first mechanism is the localization and the level of production of ATP in mitochondria. In islet β cells, glucose treatment produces the microdomain of ATP beneath the plasma membrane, which is guessed because peripherally located mitochondria are regulated differently from mitochondria in the rest of the cytosol

(Kennedy et al., 1999). Mitochondria were confirmed at the lamella in our experiments; hence, these peripheral mitochondria would produce spatiotemporal heterogeneity of ATP in HeLa cells. Another possible mechanism is the consumption of ATP by ATPase or cytoskeleton during morphological changes. As shown in Fig. 2-1b, c and Fig. 2-7b, e, i, j, ATP is consumed during actin polymerization. Additionally, since cellular morphological change accompanies the morphological change of cellular membrane, ATPase function during this process should be considered as well. For example, dynamin, known to be mainly active in membrane fission, has been discovered in various dynamic membrane structures, such as lamellipodia at the leading edge of moving cells (Buccione et al., 2004; Kruchten and McNiven, 2006). Besides dynamin, soluble N-ethylmaleimide-sensitive factor attached protein receptor (SNARE)-related proteins such as vesicle-associated membrane proteins (VAMPs) are also associated with cellular morphology in epithelial cells (Gierke and Wittmann, 2012). Being active events at the cell edge, actin dynamics and membrane morphological change could also result in ATP heterogeneity.

In summary, we explored the spatiotemporal behavior of HeLa cells in terms of ATP level change, cellular morphological change, and cytoskeletal dynamics under physiological conditions. Simultaneous imaging and detailed image processing revealed that, at the cell edge, both actin dynamics and microtubule dynamics are inextricably tied to changes in intracellular ATP levels and cellular morphology.

2.4 Materials and Methods

Materials

FM4-64 was purchased from Invitrogen, Latrunculin A was from TOCRIS, and Taxol and 2-DG was from Sigma-Aldrich.

Plasmid construction

The ATeam 1.03 plasmid was kindly provided by Dr. Imamura (Kyoto University, Kyoto, Japan). EB3-mCherry and EB3-Venus were constructed in our laboratory. EB3 was derived from Human cDNA library and amplified using PCR. PCR products were digested with BamHI and NotI, and cloned into a pcDNA3.1(+) vector inserted into mCherry or Venus at NotI and XhoI sites.

Cell culture

HeLa cells were cultured in Dulbecco's modified Eagle's medium (DMEM, Invitrogen) supplemented with 10% FBS (NICHIREI BIOSCIENCE INC) and 1% penicillin/streptomycin (Nacalai Tesque). Cells were maintained at 37 °C in a humidified atmosphere of 5% CO₂. One to two days before transfection, cells were plated at $1\sim 2 \times 10^4$ cells /cm³ onto a glass-based dish (IWAKI).

Transient transfection

Cells were transfected using lipofectamine LTX (Invitrogen), provided that construct concentrations were 1 µg/dish for ATeam, 0.5 µg/dish for EB3 probes, and 2 µg/dish for Venus-actin. After the transfection, medium was changed to Phenol red-free culture medium. Imaging was conducted 12–36 h after transfection.

Fluorescence microscopy

All fluorescent imaging experiments were performed using a confocal laser-scanning microscope (FV1000 IX81, OLYMPUS) with a ×100 oil immersion objective lens.

Furthermore, $\times 5$ optical zoom was used to focus on the cell edge. FM4-64 (200 $\mu\text{g}/\text{mL}$) was applied 50–100 $\mu\text{L}/\text{dish}$ before acquisition of the images.

In whole cell imaging, ATeam was excited by a diode laser (440 nm) through a dichroic mirror 405–440/515. The emitted fluorescence was separated by a 510 nm dichroic mirror, and signals from mseCFP and mVenus were observed at 460–500 nm and 515–545 nm, respectively.

For simultaneous imaging of ATeam and EB3-mCherry, ATeam and mCherry were excited by the diode laser (440 nm) and a helium-neon laser (559 nm), respectively, through a beam splitter 20/80. The fluorescence was separated by dichroic mirrors (510 nm and 560 nm), and signals from mseCFP, mVenus, and mCherry were observed at 475–500 nm, 510–530 nm, and 575–675 nm, respectively.

In simultaneous imaging of EB3-Venus or actin-Venus and FM4-64, Venus and FM4-64 were simultaneously excited by an argon (Ar) laser (515 nm) through a beam splitter 20/80. The emitted fluorescence was separated by a 560 nm dichroic mirror and signals from Venus and FM4-64 were observed at 535–545 nm and 620–720 nm, respectively. Images were acquired with a resolution of 640×640 pixels (actual size: 0.039 $\mu\text{m}/\text{pixel}$).

For simultaneous imaging of ATeam and FM4-64, these probes were excited by the diode laser (440 nm) and the Ar laser (515 nm), respectively, through the beam splitter 20/80. The emitted fluorescence was separated by dichroic mirrors (510 nm and 560 nm) and signals from mseCFP, mVenus, and FM4-64 were observed at 460–500 nm, 535–560 nm, and 610–710 nm, respectively. Images were acquired with a resolution of 640×640 pixels (actual size: 0.039 $\mu\text{m}/\text{pixel}$).

In whole-cell ATeam imaging and simultaneous imaging, images were acquired with a resolution of 320×320 pixels (actual size: 0.397 $\mu\text{m}/\text{pixel}$) every 5 sec. In high-resolution ATeam imaging at the cell edge, images were acquired with a resolution of 640×640 pixels (actual size: 0.039 $\mu\text{m}/\text{pixel}$) every 10 sec. During imaging, cells were maintained at 37 °C using a stage heater (TOKAI HIT).

Image processing and analysis

Images were analyzed with our original software written and developed in Matlab (MathWorks). All images were median-filtered before the following steps:

Detection of cellular morphology: Median-filtered images were binarized and labeled. Binarization was conducted by Otsu's method using Matlab. The area with the largest number of pixels was determined to be the cell (pixels to be included in the cell are called 'cell pixels').

Relative ATP level calculation: Relative ATP level was determined by calculating pixel-by-pixel mVenus/mseCFP value (called 'FRET value' below). Outlier FRET values were removed.

EB3 particle detection: A kernel large enough to contain one EB3 particle was prepared. The central pixel of the kernel was labeled 1 if the value of the pixel was more than $(\mu + \sigma)$, otherwise 0 (μ and σ refer to the average and the standard deviation of the intensities of the pixels within the kernel, respectively). Binarized images were labeled and the area with a sufficiently large size was designated as an EB3 particle. (Pixels included in an EB3 particle are called 'EB3 pixels' below.)

Unmixing processing: In analysis of simultaneous imaging, unmixing processing was conducted before calculating relative ATP levels or detecting EB3 particles. HeLa cells

expressing mseCFP, mVenus, or mCherry were prepared beforehand and any fluorescence leaked from one detection channel to another was measured for each permutation of channels under observation conditions. Then, a 3×3 matrix was derived by arranging the leakage values of each permutation. Intrinsic fluorescence was calculated by multiplying observed fluorescence by the inverse matrix of the derived matrix (Fig. 2-8).

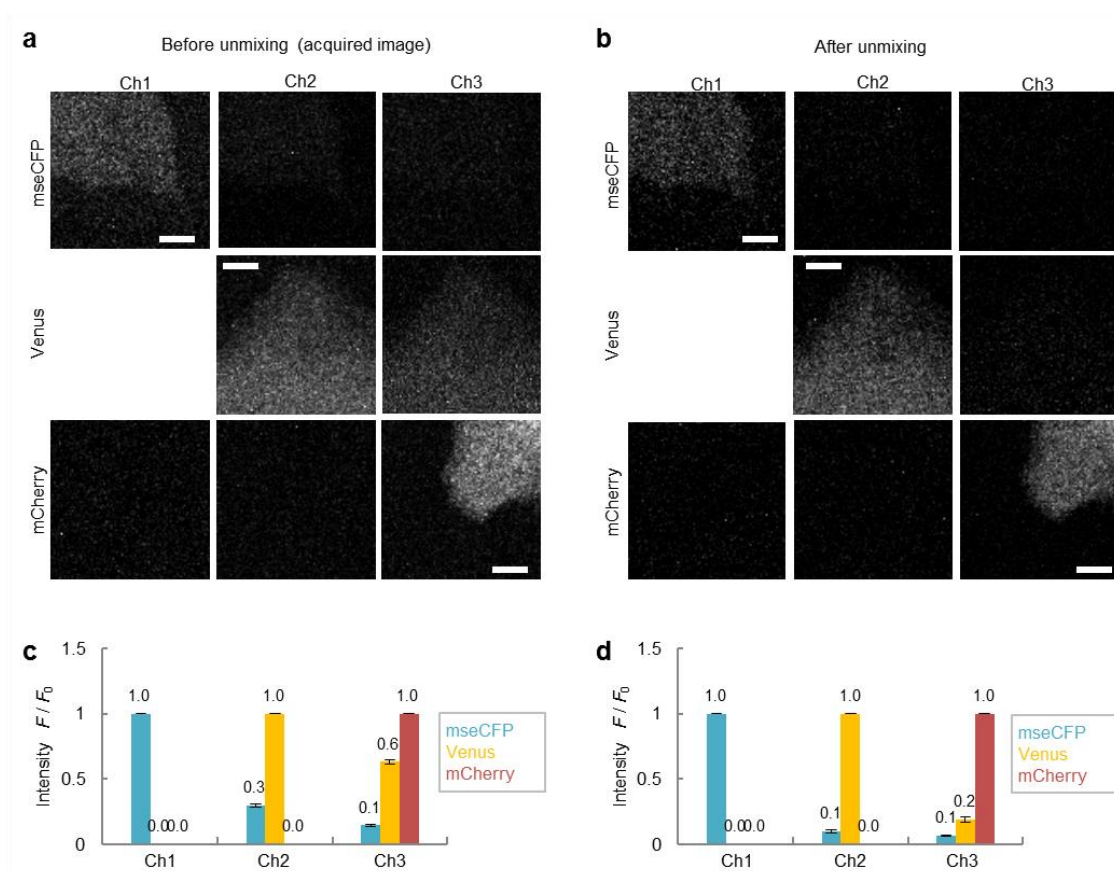


Figure 2-8. Unmixing processing.

(a, b) Typical fluorescent images of HeLa cells expressing mseCFP (upper), mVenus (middle), or mCherry (lower) acquired at Ch1 (475–500 nm), Ch2 (510–530 nm), and Ch3 (575–675 nm), before (a) and after (b) unmixing processing. Scale bar represents 5 μm . (c, d) The proportions of fluorescence consist each channels. Compared with before unmixing (c), leaked fluorescence was reduced after unmixing (d). Error bar represents SEM.

Whole cell analysis: The long axis, the short axis, and two straight lines 45 degrees to the long axis were set for cell morphology observed at $t=0$, by which the cell was sectioned into 8 compartments.

Analysis of the relationships among EB3 particle movements, cellular morphological changes, and relative ATP levels: Analysis was conducted within small, manually set ROIs at the cell edge where there are dynamic changes in morphology. EB3 density was calculated by dividing the number of EB3 pixels by the number of cell pixels. ATP level was the average of the FRET values of cell pixels. Cellular morphology at $t=t$ was subtracted from that at $t=t+1$, and the remaining pixels were considered as a newly generated cell area. To analyze how relative ATP levels behave during microtubule-related increase in the lamella area, we drew Fig. 2-6c through the following steps. First, a time window (length: 4 min) was applied to a peak in the newly generated lamella area. Second, time periods that satisfied all of the following conditions were selected: i) the peak exceeds $\mu+\sigma$ (μ and σ refer to the average and the standard deviation of the value within the time window, respectively); ii) the time window contains only one peak; iii) there is a peak in EB3 density before the peak in the newly generated lamella area; iv) the peak occurs 2 min after the start and 2 min before the end of the observation. The selected waveforms were normalized and then averaged. Finally, Fig. 2-6c was generated by averaging the waveforms after applying 5 frames of moving average.

Evaluation of the relationship between protrusion length and relative ATP levels: Raw images were first processed with median filter and background subtraction. Next, we detected cell form from averaged images of mseCFP and mVenus. The lamella area was then determined by selecting a region where a square kernel (radius: 1.75 μm) could be completely contained, and the exterior region was defined as the peripheral structure (we selected 1.75 μm because the lamella appeared to be 2 μm inside of the boundary of the peripheral structure in our observation (Fig. 2-9c); although the peripheral structure estimated by this method appears larger than the real image (Fig. 2-3), we considered

that it would have no significant impact because the differences of protrusion length are presented in Fig. 2-7). We then set a small ROI (of the same size as was used in the analysis in Fig. 2-6) at the cell edge where there are dynamic changes in morphology. Protrusion length was estimated by averaging the length of the peripheral structure. Relative ATP levels were calculated by averaging the FRET value within the area that is 2 μm inside of the boundary of the lamella (Fig. 2-9f; we determined the region to be 2 μm inside of the boundary to avoid striking changes in the region size for calculating FRET values during changes in morphology). Finally, we applied moving average (3 min before and after for physiological conditions, and 1 min before and after for inhibitor-treated conditions) to the protrusion length and relative ATP levels, and plotted the values using pseudo color.

Random shuffling: Random sequences were generated by matlab function from acquired datasets. Order of each value was shuffled.

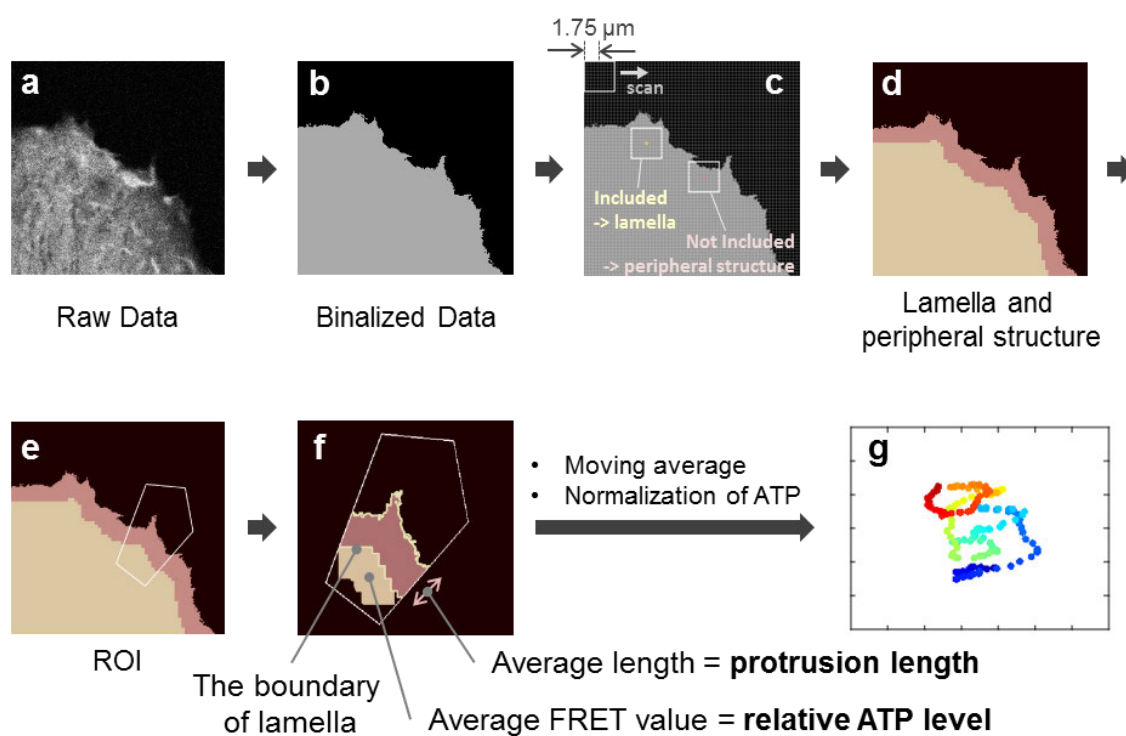


Figure 2-9. Evaluation of the relationship between protrusion length and relative ATP levels.

(a) Averaged image of mseCFP and mVenus. (b) Detected cell form. (c,d) Lamella area was determined by selecting a region where a square kernel (radius: $1.75 \mu\text{m}$) could be completely contained, and exterior region was defined as the peripheral structure. (e) A small ROI was set at the cell edge where there are dynamic changes to morphology. (f) Protrusion length was estimated by averaging the length of the peripheral structure. Relative ATP levels were calculated by averaging the FRET value within the area that is $2 \mu\text{m}$ inside of the boundary of the lamella. (g) Moving averaged values of protrusion length and relative ATP levels were plotted with pseudo color.

Statistical Analysis

To compare the relative ATP levels from before and after inhibition of cytoskeletal dynamics at the center and edge parts of the cell, we averaged the values of the 3rd–23rd pictures (15 seconds–115 seconds from the onset of observation) and that of the 97th–117th pictures (365 seconds–465 seconds from the inhibition). In Fig. 2-1, ‘center’ means the area 10–20% from the center of the cell and ‘edge’ means the area 10–20% from the cell edge. Data were evaluated by Student’s t-test or Paired t-test.

3. Chapter 3

Correlation analysis between membrane potential and ATP of mitochondria and axonal elongation

3.1 Introduction

Mitochondria are organelles that produce adenosine triphosphate (ATP), a major energy source for living bodies, and are known to be enriched in regions that have a high energy demand at both the organ and subcellular levels (Attwell and Laughlin, 2001; Lukic-Bilela et al., 2011; MacAskill and Kittler, 2010). This is especially true for neurons due to their highly polarized morphology, which is indispensable for proper neuronal activities, and local activity that requires in-place and highly effective energy production *via* mitochondria. In fact, neuronal mitochondria are enriched in specific cellular regions with large energy demands, such as synapses, nodes of Ranvier, and growth cones (GCs) (Harris et al., 2012; Saxton and Hollenbeck, 2012). Although action potential generation is known to be a major ATP consumer in neurons (Harris et al., 2012; Rangaraju et al., 2014; Sheng, 2014), morphological changes and neurite growth also require substantial amounts of energy, especially during developmental stages (Fukumitsu et al., 2015; Sheng and Cai, 2012; Spillane et al., 2013; Vaarmann et al., 2016).

Although mitochondria have a variety of roles, ATP production is considered a major function, because the inhibition of oxidative phosphorylation results in stalled mitochondria and defective neuronal behavior (Nicholls and Budd, 2000; Oruganty-Das et al., 2012; Surin et al., 2012; Tao et al., 2014; Vaarmann et al., 2016). Therefore, ATP and mitochondria are frequently considered to be closely related to cellular viability or health. For example, many neurodegenerative diseases with a loss of neuronal function and morphology have accompanying mitochondrial dysfunctions (Plucińska et al., 2012; Takihara et al., 2015; Wang et al., 2016). Additionally, in some neuronal injury

Correlation analysis between membrane potential and ATP of mitochondria and axonal elongation

models, unimpaired mitochondria are crucial for neuronal energy recovery and neuronal survive (Connolly et al., 2014; Wang et al., 2016). In this context, the existence of healthy mitochondria seems to be interpreted as sufficient ATP availability in neurons, although in most cases mitochondrial ATP (ATP_{mito}) was not measured. There are some studies showed mitochondrial activity; however, mitochondrial inner membrane potential (IMP_{mito}) was frequently investigated as surrogate measure of ATP_{mito} , despite no direct demonstration of correlation in physiological conditions between them.

Furthermore, previous findings regarding neuronal mitochondria were derived from experiments using artificial manipulation of mitochondrial functions, such as knockdown of mitochondria-specific proteins required for docking to motor proteins or for fission/fusion (Hayashi et al., 2011; Vaarmann et al., 2016; Yu et al., 2016).

However, mitochondria in neurites are regulated by multiple, complex mechanisms and several properties exhibit large variety, such as transport (direction, velocity, proportion of moving mitochondria, and anchoring or docking), distribution, fission and fusion, and morphology (size or aspect ratio), other than functional aspects such as IMP_{mito} and ATP_{mito} (Saxton and Hollenbeck, 2012; Sheng and Cai, 2012). Moreover, mutual relationships between some of these properties have recently been revealed. For example, knockdown of the fusion-related protein, optic atrophy 1 (OPA1), resulted in changes to mitochondrial size and morphology, as well as transport velocity and distribution (Yu et al., 2016). The dominant negative form of trafficking kinesin protein 2 (TRAK2), a kinesin adaptor protein, also caused defective mitochondrial transport, as well as reduced IMP_{mito} (Fukumitsu et al., 2015). Furthermore, a consensus regarding a mutual relationship between IMP_{mito} and direction of transport has not been established. Miller and Sheetz suggested that 90% of mitochondria with high IMP_{mito} move anterogradely, whereas 80% of those with low IMP_{mito} move retrogradely (Miller and Sheetz, 2004), while another study showed no correlation between IMP_{mito} and the direction of axonal transport (Verburg and Hollenbeck, 2008). Due to the mutual dependency and complexity of several mitochondrial properties, it is necessary to study

Correlation analysis between membrane potential and ATP of mitochondria and axonal elongation

mitochondrial function without artificial interruption to clarify native mitochondrial behavior.

To clarify native mitochondrial behavior, especially regarding energy metabolism abilities, direct measurements of ATP_{mito}, IMP_{mito} and other properties such as transport, morphology or distribution under physiological condition are necessary. Although mitochondrial isolation (Shibata et al., 2015) is one of effective methods for characterization of a mitochondrion, some property such as transport or distribution need to be measured within cells. However, little research has been conducted investigating ATP_{mito} measurements under physiological conditions or with other mitochondrial parameters in living cells. There are several reasons for this: 1) there are limited methods to directly measure ATP_{mito} with high spatiotemporal resolution (Imamura et al., 2009; Nakano et al., 2011); 2) in general, change in ATP levels without extensive stimulation is subtle, and therefore hard to evaluate; and 3) assessing a variety of properties simultaneously requires elaborate and careful preparation, conditioning and treatment in both experimentation and analysis. However, we recently used spatiotemporal image processing analysis to overcome such problems and have demonstrated relationships between biological signals collected from simultaneous fluorescent imaging under physiological conditions (Kobayashi et al., 2013; Suzuki et al., 2015).

With this background, we conducted simultaneous fluorescent imaging of ATP_{mito}, IMP_{mito}, and other mitochondrial or neuronal properties in neurons using mitAT1.03 (Imamura et al., 2009; Kioka et al., 2014; Yoshida et al., 2017), an ATP_{mito} indicator, and tetramethylrhodamine ethyl ester (TMRE) (O'Reilly et al., 2003; Zhou et al., 2014), an IMP_{mito} indicator, in this present study. Detailed analysis of the relationships revealed that not all ATP_{mito} and IMP_{mito} correlated accurately, and as for axonal elongation, ATP_{mito} is more a dominant factor than IMP_{mito}.

3.2 Results

IMP_{mito} and ATP_{mito} in transport

Firstly, to investigate ATP_{mito} or IMP_{mito} dependency on transportation, we compared ATP_{mito} or IMP_{mito} among anterogradely transported, stationary and retrogradely transported mitochondria within axonal processes using kymographs (Figs. 3-1, 3-2, 3-3). Mitochondria that moved anterogradely had relatively higher levels of ATP_{mito}; however, the difference was not significant. IMP_{mito} was relatively depolarized in retrogradely transported mitochondria compared to anterogradely transported mitochondria. However, there was no significant difference between the IMP_{mito} of anterogradely transported mitochondria and stationary mitochondria. No ATP_{mito} or IMP_{mito} dependence on mitochondrial velocity and transported distance was found (Fig. 3-4). Results of ATP_{mito} and IMP_{mito} were expected to be similar; however, our result showed that they did not accurately coincide.

Correlation analysis between membrane potential and ATP of mitochondria and axonal elongation

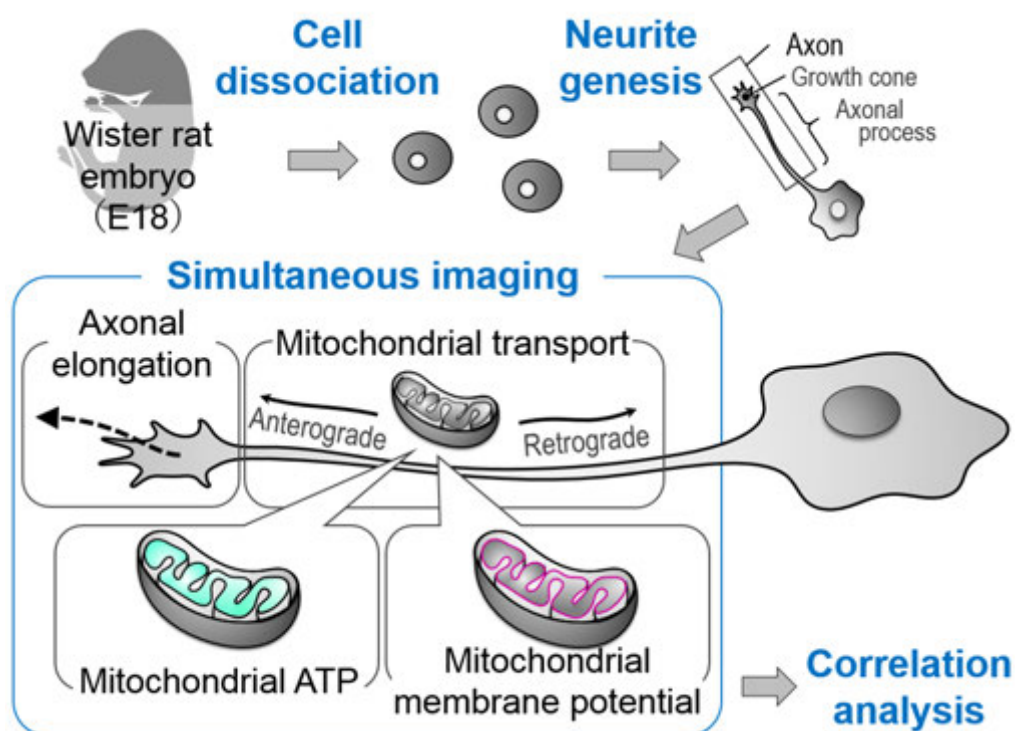


Figure 3-1. Experimental procedure of this study.

We dissociated and cultured dorsal root ganglion neurons from day 18 rat embryos and observed their mitochondrial dynamics along with axonal elongation.

Correlation analysis between membrane potential and ATP of mitochondria and axonal elongation

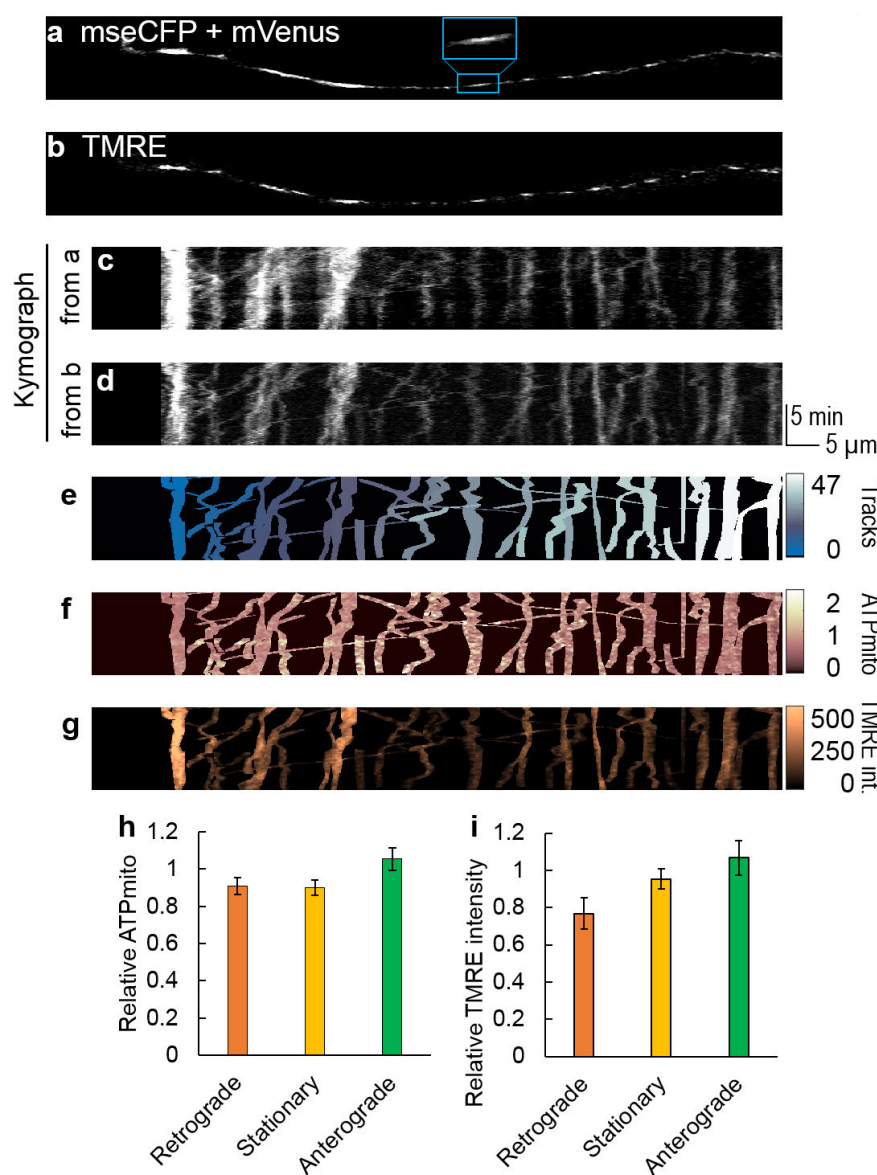


Figure 3-2. Mitochondrial ATP and inner-membrane potential dependency on the transport direction of mitochondria.

A typical image of a nerite visualized for (a) mseCFP + mVenus fluorescence (mitAT1.03) or (b) TMRE. Acquired kymograph from a (c) and b (d). (e) Manually identified mitochondrial tracks. Here, the growth cone area was excluded from kymograph. (f) Mitochondrial ATP or (g) TMRE intensity visualized in pseudo color. Each color table is linear and covers the full range of the data. Relative (h) mitochondrial ATP and (i) TMRE intensity levels for 33 retrograde, 78 stationary and 27 anterograde mitochondria from 50 axonal processes. Error bars represent the standard error of the mean (SEM).

Correlation analysis between membrane potential and ATP of mitochondria and axonal elongation

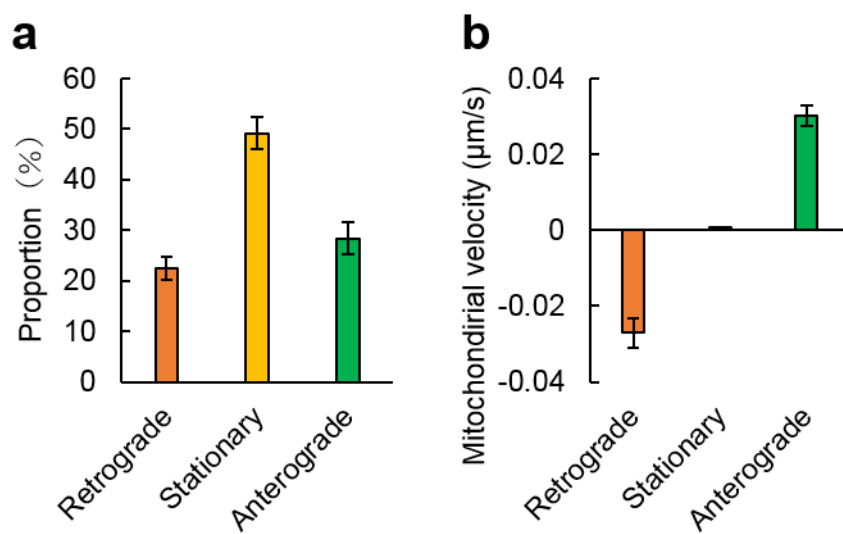


Figure 3-3. Detail characterization of mitochondria.

Average mitochondrial (a) proportions, and (b) velocity for 33 retrograde, 78 stationary, and 27 anterograde mitochondria from 50 neurons. Error bars represent SEM.

Correlation analysis between membrane potential and ATP of mitochondria and axonal elongation

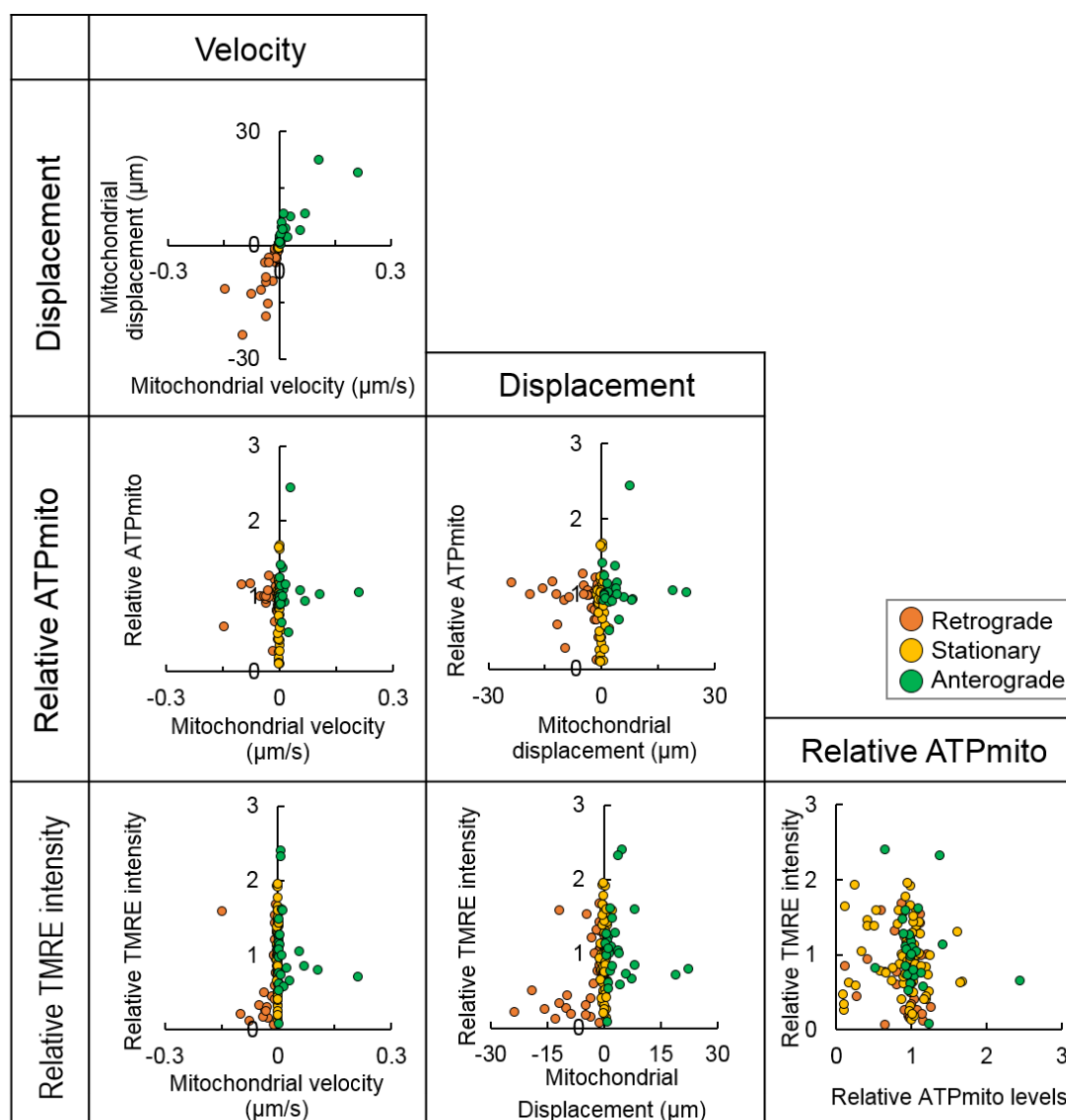


Figure 3-4. Correlation between parameters characterizing mitochondria.

Correlations of mitochondrial velocity, displacement, relative mitochondrial ATP, and relative TMRE intensity were investigated. No obvious correlation was found except the natural correlation between velocity and displacement.

IMP_{mito} and ATP_{mito} in fission/fusion

In addition to transported mitochondria, some mitochondria underwent fusion or fission events during observations. Using kymograph, we explored ATP_{mito} and IMP_{mito} behavior during fusion or fission events. During fusion events, IMP_{mito} more polarized in a post-fusion mitochondrion compared to the average of the two pre-fusion mitochondria (Fig. 3-5, left). Likewise, ATP_{mito} in a post-fusion mitochondrion were higher than the average of the two pre-fusion mitochondria (Fig. 3-5, left). During fission events, there was a difference in IMP_{mito} between the two post-fission mitochondria. Then, we compared the changes in IMP_{mito} and ATP_{mito} in both of the two post-fission mitochondria, respectively: one with a relatively highly polarized and the other with a relatively less polarized IMP_{mito} (named Post-1 and Post-2 in Fig. 3-5, right, respectively). During fission events, the IMP_{mito} of Post-2 was less polarized than that of the pre-fission mitochondrion as previously reported (Twig et al., 2008), while that of Post-1 was the same as that of a pre-fission mitochondrion (Fig. 3-5, right); however, no ATP_{mito} changes were observed. This result also indicated that ATP_{mito} and IMP_{mito} are not always behave similarly.

Correlation analysis between membrane potential and ATP of mitochondria and axonal elongation

IMP_{mito} and ATP_{mito} in distribution

We next assessed mitochondrial density using still images (Fig. 3-6). Mitochondrial density was defined as: (sum of area dominated by all mitochondria) / (area size of GC or axonal process). We confirmed that mitochondrial density was higher in the GCs compared to the axonal process (Fig. 3-7a). Although average ATP_{mito} were slightly lower in the GCs compared to the axonal process, integrated ATP_{mito} signals (calculated by multiplying average ATP_{mito} and mitochondrial density) were high in the GCs due to the high mitochondrial density (Fig. 3-7b, c). Average IMP_{mito} relatively hyperpolarized in the GCs than in the axonal process (Fig. 3-7d).

ATP_{mito} in GCs and axonal elongation have a positive correlation

Because GC is a structure related to axonal elongation, we quantified the distance of axonal elongation, and examined the role of mitochondrial dynamics in elongation. Among neurons grown during 10 min observation, the distance of axonal elongation and ATP_{mito} or integrated ATP_{mito} signals in the GCs showed a positive correlation (Fig. 3-7e, f). This correlation was stronger in GCs than in axonal processes (Fig. 3-7h, i, k, l). Furthermore, no correlation was found between elongation and IMP_{mito} for both GCs and axonal processes (Fig. 3-7g, j, m). These results suggest that ATP_{mito} in GCs, but not IMP_{mito} in GCs, contribute to axonal elongation.

Correlation analysis between membrane potential and ATP of mitochondria and axonal elongation

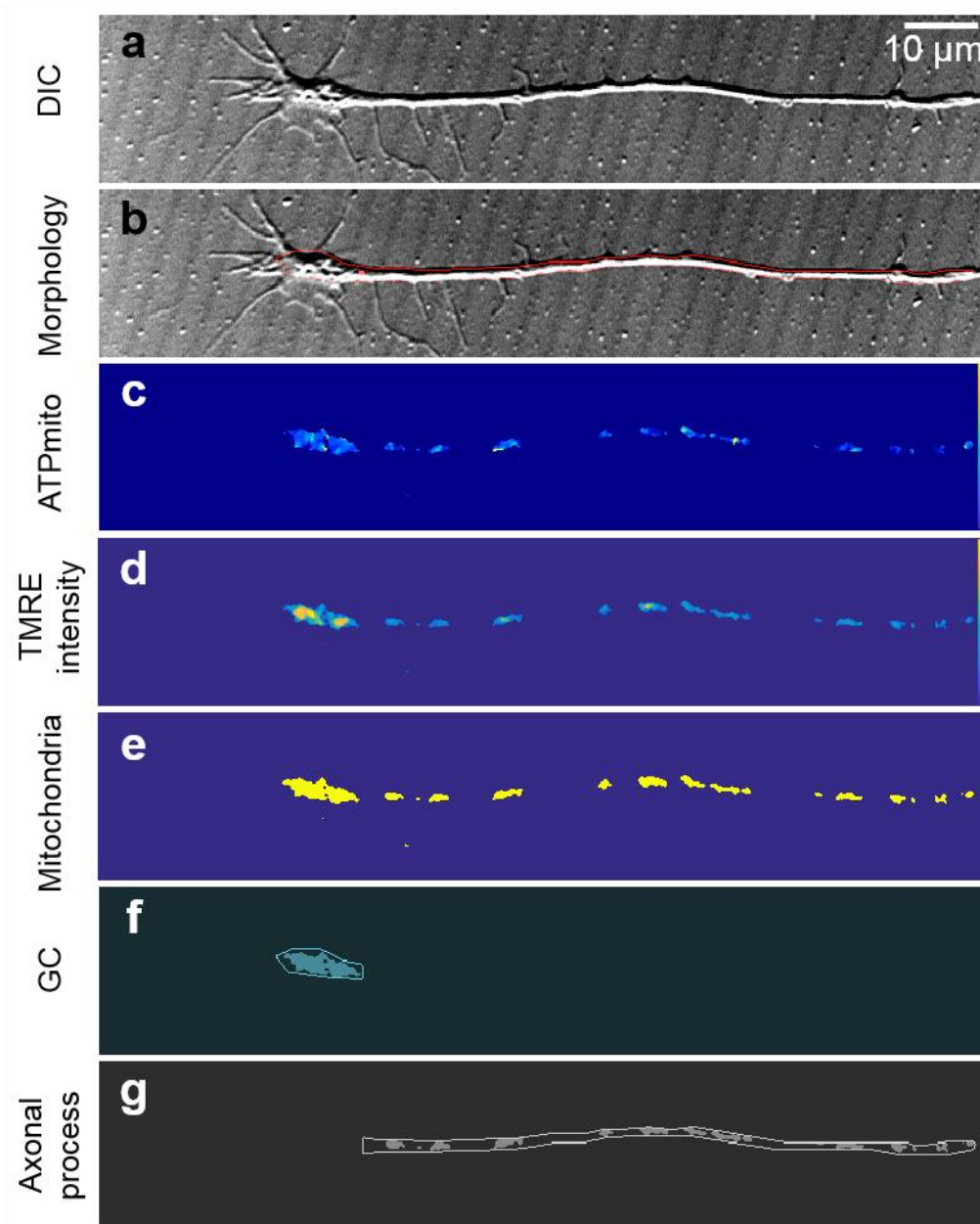


Figure 3-6. Comparison of mitochondrial properties between GC and axonal process using still images.

(a) Differential interference contrast (DIC) image of a typical neuron. (b) Red line indicates detected morphology of growth conal central (C-) domain and axonal process. A neck of GC represented by a red point was manually defined. Pseudo color image of (c) mitochondrial ATP levels and (d) TMRE intensity. (e) Detected mitochondria. Morphology of the area and mitochondrial location within the area indicated for both (f) GC and (g) axonal process.

Correlation analysis between membrane potential and ATP of mitochondria and axonal elongation

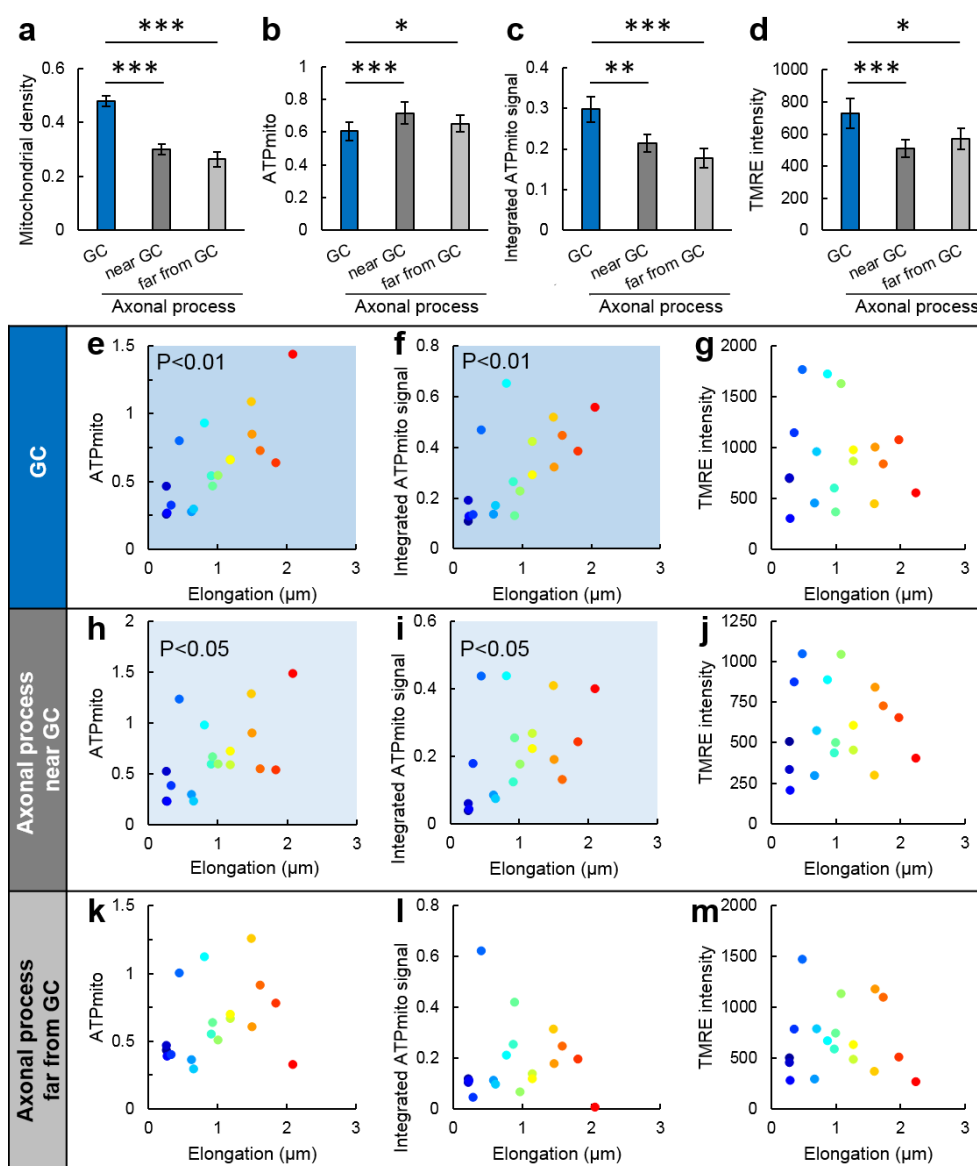


Figure 3-7. Mitochondria in GCs and axonal processes show different correlations between axonal elongation and mitochondrial ATP or inner-membrane potential.

Average (a) density, (b) mitochondrial ATP levels, (c) integrated mitochondrial ATP signals (density \times mitochondrial ATP levels), and (d) TMRE intensity of growth cones (GC; blue), axonal processes near GCs (0–20 μm from GC; grey) and axonal processes relatively far from GCs (20–40 μm from GC; light grey). Correlations between the distance of axonal elongation with (e, h, k) mitochondrial ATP, (f, i, l) integrated mitochondrial ATP signal or (g, j, m) TMRE intensity at (e–g) GCs, (h–j) axonal processes near GCs and (k–m) axonal processes relatively far from GCs. Data were taken from (a–d) 29 neurons or (e–m) a subset of 18 neurons grown from within those 29 neurons. In (e–m), each color represents each neuron. Error bars represent SEM.

Correlation analysis between membrane potential and ATP of mitochondria and axonal elongation

ATP_{mito} in GCs are involved in axonal elongation and GC morphological change

To verify the importance of ATP_{mito} in GCs for elongation, we further examined the effect of artificially disrupting IMP_{mito} or ATP_{mito} on axonal elongation using a mitochondrial uncoupler, carbonyl cyanide-p-trifluoromethoxyphenylhydrazone (FCCP), or the ATP synthase inhibitor, Oligomycin A, respectively.

Both FCCP and Oligomycin A induced apparent drawing back of neurons compared to the control condition (i.e., neurons without drug treatment; Fig. 3-8a–c). However, the detail of change in IMP_{mito} and ATP_{mito} differed between FCCP and Oligomycin A, as well as between GCs and axonal processes. In GCs treated with FCCP, IMP_{mito} depolarized and ATP_{mito} decreased, and the declines correlated with axonal drawing backs (Fig. 3-8d, upper). On the other hand, in axonal processes treated with FCCP, although IMP_{mito} depolarized, ATP_{mito} did not significantly change (Fig. 3-8d, lower). As a result, no correlation was observed in axonal processes between the decrease in ATP_{mito} and axonal drawing back. Although drawing back and depolarization of IMP_{mito} showed a correlation in axonal processes, the peak was lower than that in GCs. After treatment with Oligomycin A, ATP_{mito} decreased both in GCs and in axonal processes; however, IMP_{mito} levels did not change for either GCs or axonal processes (Fig. 3-8e). Therefore, no correlation was found between IMP_{mito} and drawing back while there was a correlation between the decrease in ATP_{mito} and drawing back. Again, the correlation was more remarkable in GCs.

Axons drew back even when IMP_{mito} did not depolarized (Fig. 3-8c–e). Additionally, axonal drawing back correlated more with the decrease in ATP_{mito} than in IMP_{mito}, and this correlation was higher in GCs than in the axonal processes. These results again indicated that ATP_{mito}, especially in GCs, are crucial for axonal elongation.

Correlation analysis between membrane potential and ATP of mitochondria and axonal elongation

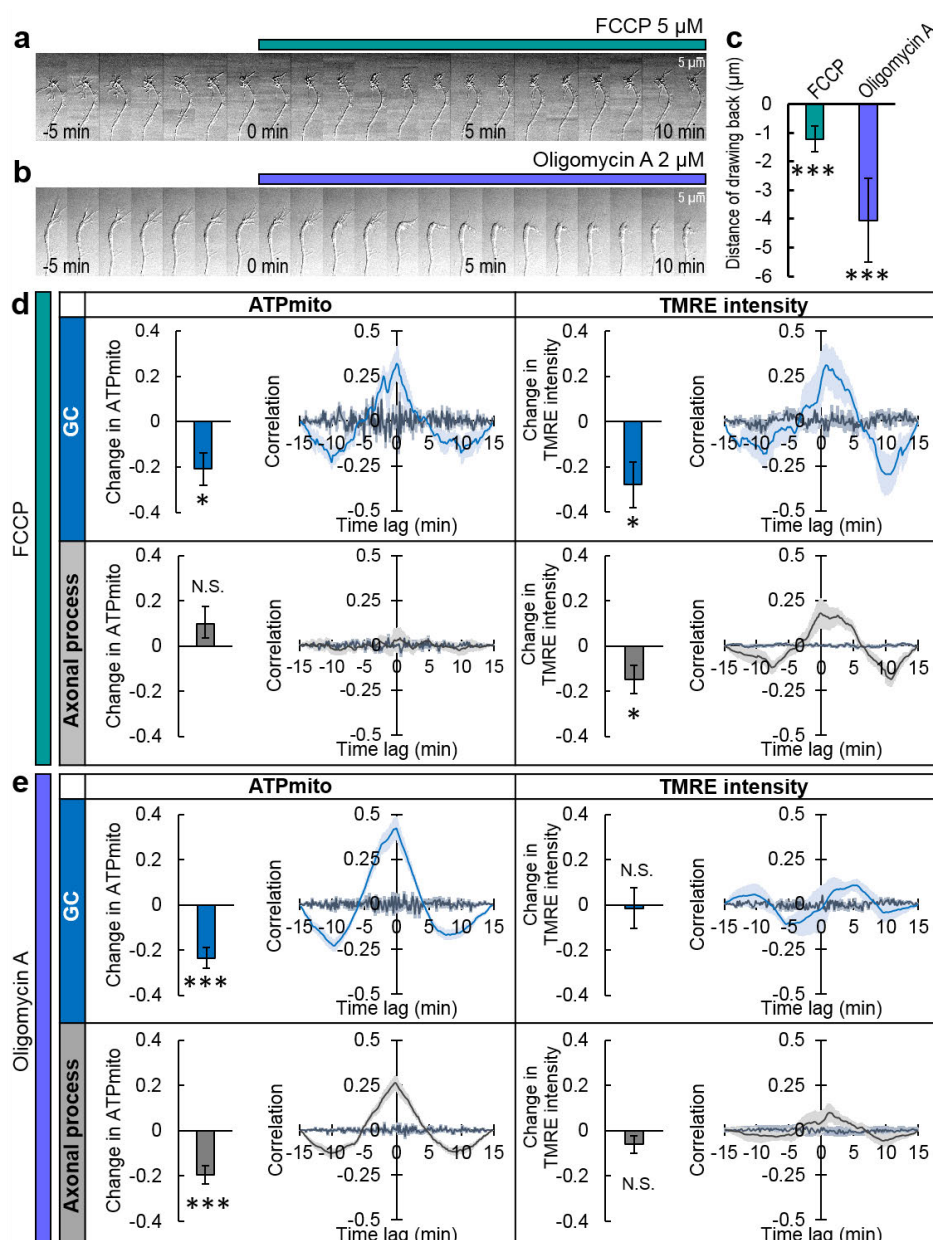


Figure 3-8. Mitochondrial ATP in GCs had a correlation with axonal dynamics.

Typical images of axons treated with (a) 5 μM FCCP or (b) 2 μM Oligomycin A. (c) Average distance of axonal drawing back after treatment of FCCP or Oligomycin A. Average changes and cross-correlation functions with drawing back of (left) mitochondrial ATP levels or (right) TMRE intensities when axons were treated with (d) FCCP (7 axons) or (e) Oligomycin A (11 axons). In figures of average changes, error bars represent SEM. In figures showing cross-correlation functions, blue lines (in upper rows), grey lines (in lower rows), and dark-blue lines (in all figures) represent correlations calculated in GCs, in axonal processes, and from random-shuffled datasets, respectively. Light-shaded bars attached to the lines represent SEM.

In addition to axonal process drawing back, GC collapse was observed. To examine this change quantitatively, we conducted additional analyses of the changes in GC morphology, with a focus on the effect of Oligomycin A because it induced more drastic morphological changes than FCCP. The indices that we quantified were (i) area, (ii) newly appeared area, (iii) newly disappeared area, (iv) the sum of the newly appeared area and the newly disappeared area, (v) edge length and (vi) the ratio of edge length to area of both the peripheral- (P-) and the central- (C-) domains of the GC (Fig. 3-9). The (ii) newly appeared area, (iii) newly disappeared area and (iv) their sum in the P-domain correlated positively with axonal drawing back after treatment with Oligomycin A. This means that these indices decreased along with drawing back of the axonal process. The (i) area of the C-domain and the (v) edge length of both the P- and C-domains exhibited peaks before (negative time lag values) and after (positive time lag values) drawing back. This means that axonal drawing back occurred after the C-domain area decreased (the positive peak at negative time lag), and that the C-domain area relatively increased after drawing back (the negative peak at positive time lag). Peaks in the (v) edge length and (vi) ratio of edge length to area of the P-domain shows that the P-domain attains a less protrusive morphology before axonal drawing back. The (v) edge length of the C-domain increases just after drawing back, which can be attributed to the crumpling of the C-domain when normal intact morphology collapses.

Correlation analysis between membrane potential and ATP of mitochondria and axonal elongation

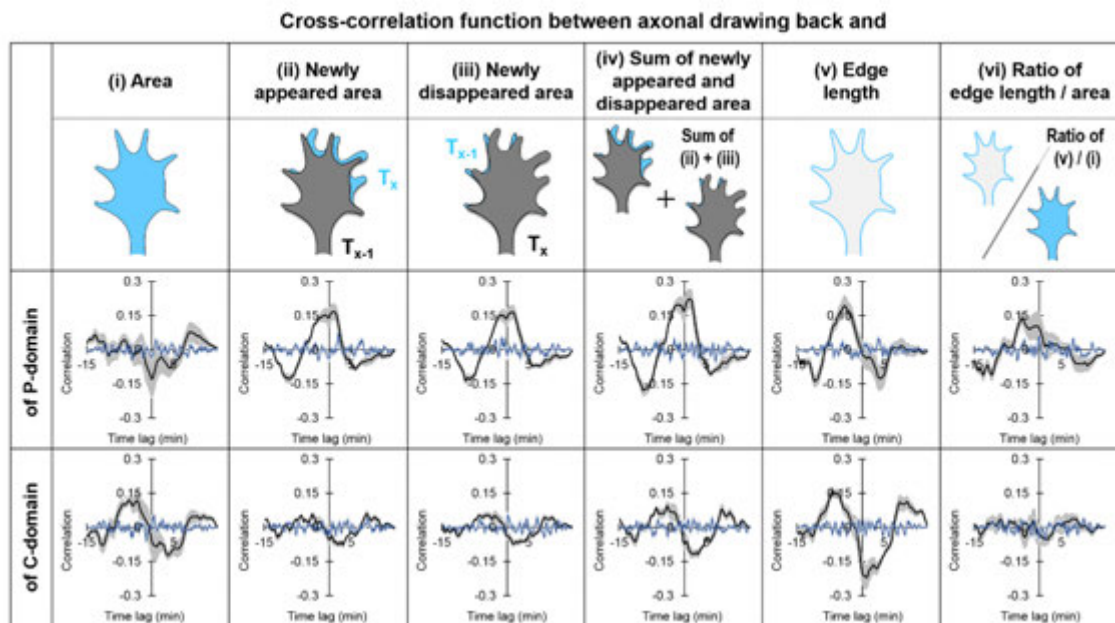


Figure 3-9. Correlation between changes in GC morphology and axonal process dynamics.

Cross-correlation function between neck position drawing back and each index of GC morphology (black lines). Blue lines represent cross-correlation function derived from randomly shuffled datasets. Both the black and blue lines are the averaged results from 11 neurons. The horizontal axis represents time lag (min), and the vertical axis represents correlation. Light-shaded bars attached to the lines represent SEM.

Correlation analysis between membrane potential and ATP of mitochondria and axonal elongation

Moreover, correlation analysis between these indices and ATP_{mito} revealed that the (ii) newly appeared area, (iii) the newly disappeared area and (iv) their sum in the P-domain correlated positively with ATP_{mito} in the GC (Fig. 3-10). Importantly, none of these indices correlated in the C-domain or the axonal process. These results indicate that although ATP_{mito} decrease and axonal drawing back were positively correlated (Fig. 3-8e), analysis focused on GC morphology revealed that ATP downregulation manifested as less dynamic morphological changes in the P-domain of the GC. Because morphological changes in the P-domain relies mainly on actin dynamics, these results suggest the importance of ATP in actin turnover in GCs.

Correlation analysis between membrane potential and ATP of mitochondria and axonal elongation

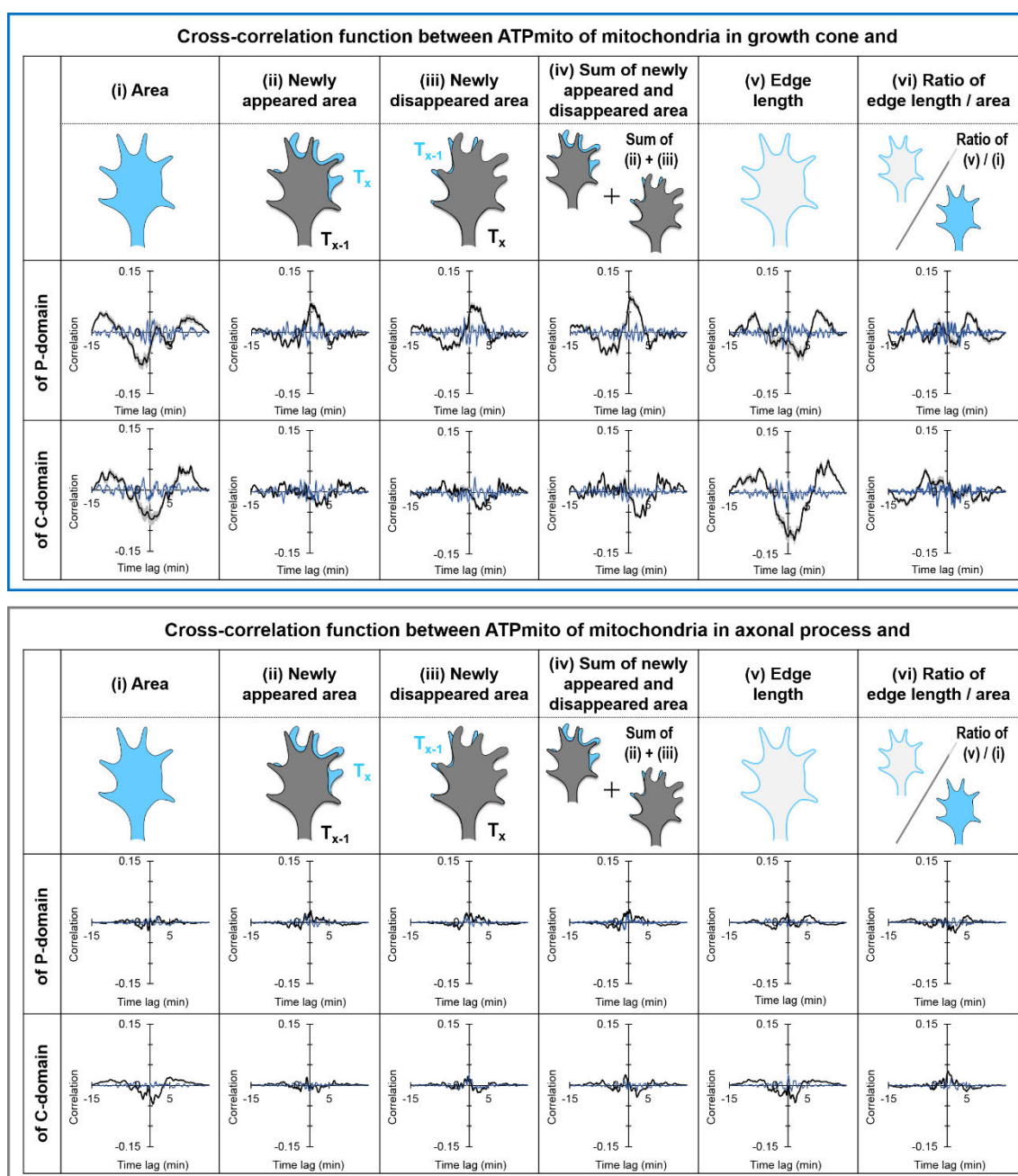


Figure 3-10. Correlation between changes in GC morphology and mitochondrial ATP.

Cross-correlation function between changes in mitochondrial ATP and each index of GC morphology (black lines) in either GC mitochondria (upper) or axonal process mitochondria (lower). Blue lines represent cross-correlation function derived from randomly shuffled datasets. Both the black and blue lines are averaged results from 11 neurons. The horizontal axis represents time lag (min), and the vertical axis represents correlation. Light-shaded bars attached to the lines represent SEM.

Actin turnover is one processes related to neuronal ATP dynamics

To clarify the relevance of actin dynamics, we explored the changes in the GC morphology and cytosolic/mitochondrial ATP levels in response to treatment with Latrunculin A, an inhibitor of actin turnover (Fig. 3-11). Latrunculin A treatment led to a decrease in the number of newly appeared area in the P-domain, but not the C-domain (Fig. 3-11a). Latrunculin A treatment caused no change in ATP_{mito} (Fig. 3-11d); however, cytosolic ATP levels increased both in the P- and C-domains (Fig. 3-11b). Thus, this increase in cytosolic ATP is not because of enhancement of mitochondrial ATP, but may be because of suppression of actin turn over caused by Latrunculin A. Importantly, the increase in cytosolic ATP and the decrease in P-domain area were positively correlated (Fig. 3-11c). The above indicates that actin turnover is a potential mechanism producing the correlation between ATP and neuronal dynamics.

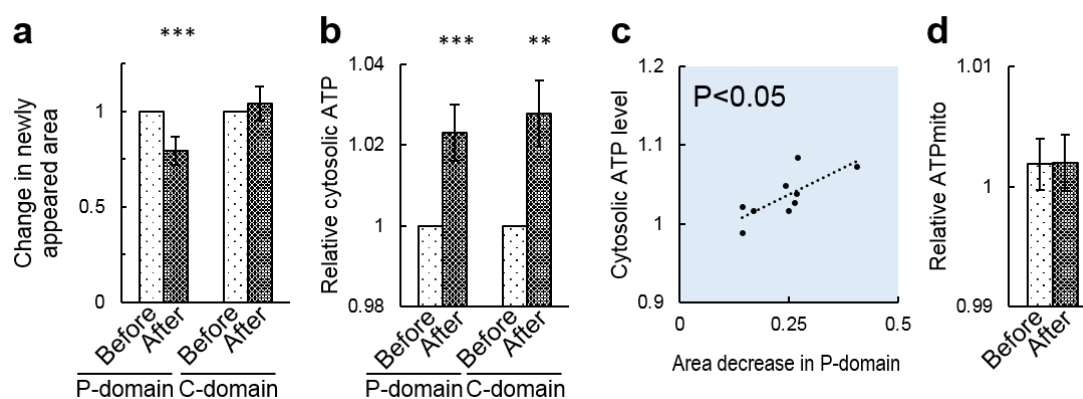


Figure 3-11. Effects of inhibition of actin turnover on GC dynamics.

(a, b) Quantitative analyses of changes in (a) newly appeared area and (b) cytosolic ATP levels before and after treatment with Latrunculin A ($n = 9$). Latrunculin A decreased newly appeared areas in only the P-domain, whereas cytosolic ATP levels increased in both the P- and C-domains. (c) Correlation between the degree of decrease in the P-domain area and the increase in cytosolic ATP level in GCs. (d) Comparison of mitochondrial ATP before and after Latrunculin A treatment ($n = 5$). Mitochondrial ATP was not altered by Latrunculin A treatment. Error bars represent SEM.

Correlation between ATP_{mito} and IMP_{mito}

Although ATP_{mito} and IMP_{mito} showed similar trends in some cases, different behavior was found during transport, fission/fusion and axonal elongation. To investigate the relation of them in more detail, we visualized IMP_{mito} and ATP_{mito} over time (Fig. 3-12a). Each track was classified as i) a positive correlation, ii) a negative correlation, iii) changing with time (drawing circle either clockwise or anti-clock wise), iv) no correlation, or v) other. Tracks classified as (iii) were further divided into eight parts by every 90 degree for both clockwise and anti-clockwise rotation directions. Here, clockwise rotation represents ATP_{mito} following IMP_{mito} and *vice versa* (Fig. 3-13). Concurrently, cross-correlation functions between IMP_{mito} and ATP_{mito} were calculated. Typical wave-forms of the cross-correlation function are illustrated for i), ii), iv), v) and for the eight parts of iii) in Fig. 3-13. These results show that IMP_{mito} and ATP_{mito} are not necessarily correlated, although we cannot exclude the possibility that this is because of differences in the ability of the two probes to detect changes in each signal.

Considering the frequency of each type of events, it is understandable that an average of cross-correlation functions between ATP_{mito} and IMP_{mito} of all mitochondria showed a delayed positive peak (ATP_{mito} changed following IMP_{mito} change; Fig. 3-12b). The observed peak was statistically significant as randomly-shuffled data did not show a peak (Fig. 3-12b).

Correlation analysis between membrane potential and ATP of mitochondria and axonal elongation

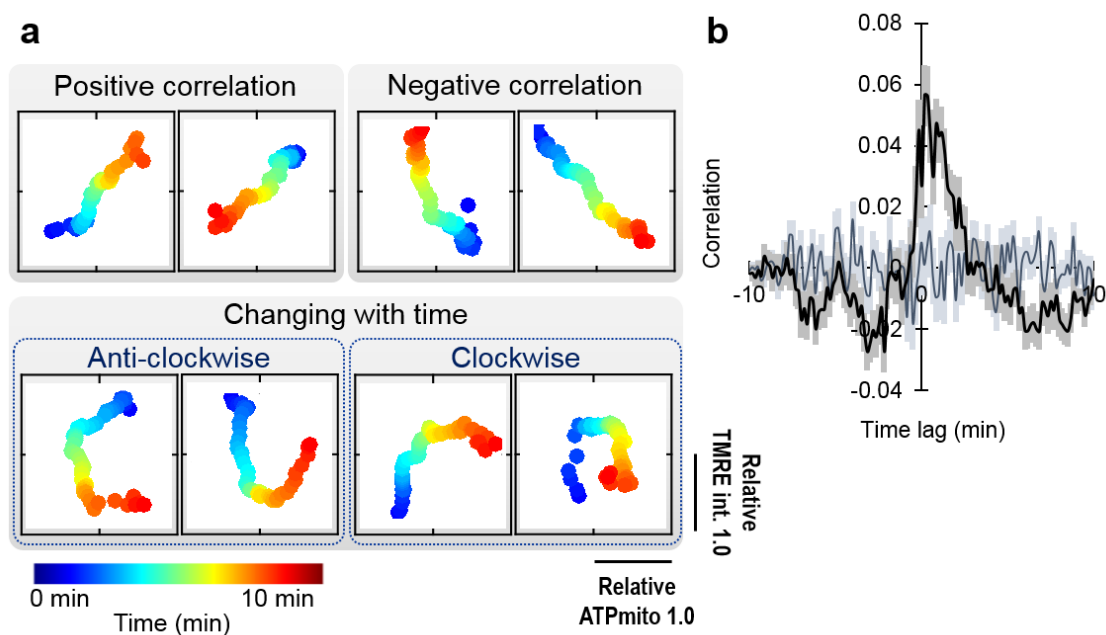


Figure 3-12. Mitochondrial ATP and inner-membrane potential do not always correlate.

(a) Representative examples of transitions in TMRE intensity (vertical axis) and mitochondrial ATP levels (horizontal axis) in each mitochondrion. Time is represented by a pseudo-color scale, which is linear and fully covers the data range. (b) Cross-correlation function between TMRE intensity and mitochondrial ATP levels. Average (black line) and SEM (grey bars) are indicated for 371 mitochondria from 50 axonal processes. The dark blue line and light blue soft-shaded bars represent the average and SEM of correlations calculated from randomly shuffled datasets, respectively.

Correlation analysis between membrane potential and ATP of mitochondria and axonal elongation

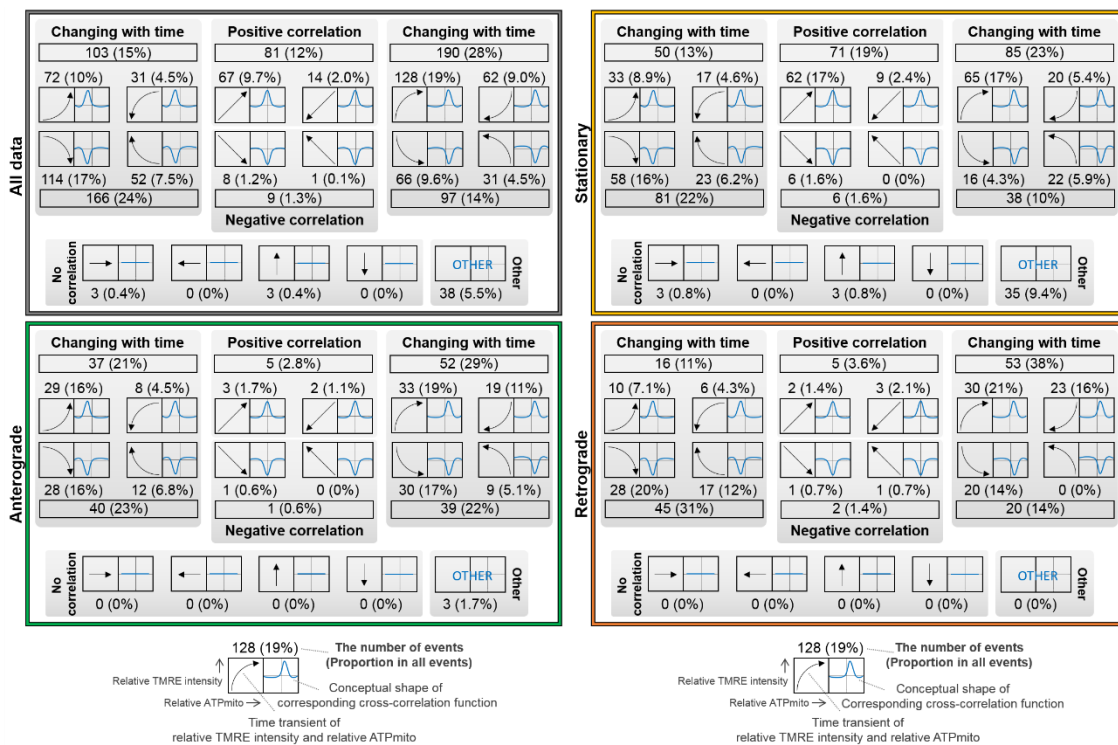


Figure 3-13. Detailed trajectories of TMRE intensity and mitochondrial ATP levels.

Illustrated time transients, the conceptual shapes of corresponding cross-correlation functions, and the numbers and proportions of each type of mitochondrial track from 50 neurons.

3.3 Discussion

We conducted simultaneous imaging and spatiotemporal analyses of ATP_{mito} and IMP_{mito} during mitochondrial transport, fission/fusion and axonal elongation. We demonstrated that ATP_{mito} and IMP_{mito} are not always accurately correlated, and for axonal elongation, ATP_{mito} is a more dominant factor than IMP_{mito}.

The role of mitochondria in axonal elongation has been reported previously; mitochondrial transport responds to axonal outgrowth or growth factors (Chada and Hollenbeck, 2003; Chada and Hollenbeck, 2004), and the number and positioning of mitochondria is related to neurite elongation (Fukumitsu et al., 2015; Spillane et al., 2013; Tao et al., 2014; Vaarmann et al., 2016). These reports suggest that mitochondrial localization and ATP generation are crucial for axonal elongation. Although some of these previous studies measured cytosolic ATP levels directly or indirectly, no report has explored native ATP_{mito} under physiological conditions. In this study, we successfully demonstrated a correlation between ATP_{mito} within GCs with axonal elongation under physiological conditions.

Our results are also consistent with recent research demonstrating the importance of cytosolic ATP in the cellular motility of non-neuronal cells (De Bock et al., 2013; Suzuki et al., 2015). These studies explored cytosolic ATP, not ATP_{mito}, possibly because these cell types have greater dependency on glycolysis compared to others (Groschner et al., 2012; Ward and Thompson, 2012). Nevertheless, this study is one of the few that measured mitochondrial/cytosolic ATP itself to demonstrate their relevance in cellular morphological changes.

We have found that ATP_{mito} and IMP_{mito} are not necessarily correlated under physiological conditions. Some background phenomena may have contributed to this discrepancy. Firstly, differences in the ability of two probes to detect changes in each signal could obscure any potential correlation. Secondly, there is a possibility that the ATP_{mito} value reflects an accumulative IMP_{mito} value up to that time, instead of IMP_{mito}

at the time, because IMP_{mito} at any given time is simply the difference in voltage in the mitochondrial inner membrane. On the other hand, ATP_{mito} has been considered to represent the net ATP pool in mitochondria at a given time. ATP_{mito} and summation of IMP_{mito} also positively correlated, and the correlation peak was highest when the IMP_{mito} summation period was approximately 2 min (Fig. 3-14a). However, the 2 min period was an average, and the duration at which the strongest correlation was observed differed depending on each individual mitochondrion (Fig. 3-14b). This may be because ATP_{mito} is a result of not only production, but also consumption and flux from the mitochondrial matrix. IMP_{mito} is generally considered an index linked to ATP_{mito} production, and the ATP_{mito} measured in this present study is a result of production and consumption/efflux. Thus, a decrease in the ATP_{mito} signal can be the result of either a reduction of ATP_{mito} production or an increase in ATP_{mito} consumption/efflux. This could also contribute to discrepancies in the correlation between the ATP_{mito} and IMP_{mito} signals.

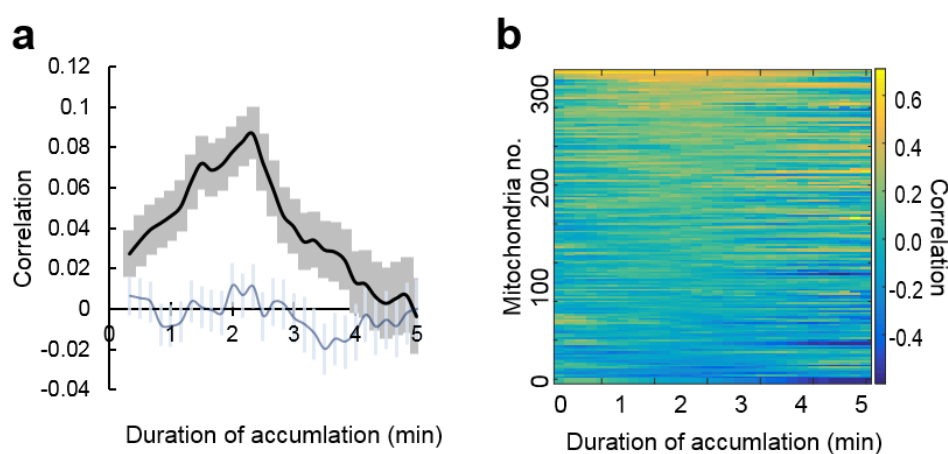


Figure 3-14. Detailed analysis of mitochondrial ATP and TMRE intensity.

(a) Cross-correlation function between accumulative TMRE intensities and mitochondrial ATP. A blue line represents cross-correlation function derived from randomly shuffled datasets. Light-shaded bars attached to the lines represent SEM. (b) Details of the correlation analysis. The width of the time period with the strongest correlation between mitochondrial ATP and accumulative TMRE intensity differ in each individual mitochondrion.

Correlation analysis between membrane potential and ATP of mitochondria and axonal elongation

Moreover, activities of electron transport chain (ETC) and ATP synthase activity are known to be flexible. Post-translational acetylation is one of the most representative modulations of mitochondrial activity. NADH:ubiquinone oxidoreductase subunit A9 (NDUFA9), an ETC complex I component, is known to be acetylated, which decreases ATP levels (Ahn et al., 2008). ATP synthase is also known to be acetylated (Rardin et al., 2013); however, this is only one facet of ATP synthase regulation, and ATP synthase activity is also under control of adenosine diphosphate (ADP) inhibition (Vasilyeva et al., 1982) or ATP synthase inhibitor (IF₁) (Gledhill et al., 2007; Pullman and Monroy, 1963; Smith et al., 1975).

In addition to direct effects on ETC or ATP synthase, there are other effectors that mediate IMP_{mito} and ATP_{mito} levels. The most well-known phenomenon involves proton leak *via* uncoupling protein (UCP) (Nedergaard et al., 2005), which diminishes the correlation between IMP_{mito} and ATP_{mito} by decreasing the number of protons that pass through ATP synthase.

Besides UCP-mediated uncoupling, mitochondrial permeability transition (MPT) (Haworth and Hunter, 1979) is another major phenomenon caused by mitochondrial permeability transition pores (PTP) (Haworth and Hunter, 1979). A PTP is a structure consisting of adenosine nucleotide translocase (ANT; translocator of ATP/ADP in mitochondrial inner membrane), voltage-dependent anion channel (VDAC; also called porin; a pore located at the mitochondrial outer membrane) and cyclophilin D (Srinivasan, 2015). The opening of PTP increases the permeability of mitochondrial membranes to molecules including proton, ATP and ADP (Rostovtseva and Colombini, 1997). Appropriate ATP/ADP translocation is essential for ATP_{mito} production in matrix, and MPT leads to loss of IMP_{mito}; thus, opening of PTP would disrupt the balance between ATP_{mito} and IMP_{mito} under physiological conditions. Furthermore, MPT is known to be induced without PTP; rapid depolarization depending on the net translocation of protons from matrix to the intermembrane space has been reported in isolated mitochondria (Hattori et al., 2005).

Previous biochemical research on mammalian oxygen consumption by mitochondria in the standard state suggested that approximately 20% was uncoupled by mitochondrial proton leak and 80% was coupled to ATP synthesis (Rolfe and Brown, 1997). Recently, a positive feedback mechanism that alters the response of IMP_{mito} to glucose concentrations was reported (Gerencser et al., 2017), and the working condition of the mitochondrial uncoupling protein also differed with regards to IMP_{mito} (Klotzsch et al., 2015). Clockwise or anti-clockwise trajectories of ATP_{mito} and IMP_{mito} also suggest that the relation between them is not linear, but rather influence each other, and the extent of the influence changes with time and condition.

In summary, we conducted simultaneous imaging of several mitochondrial properties in neurons. Detailed spatiotemporal image processing directly showed that the affect of native IMP_{mito} and ATP_{mito} are mutual; therefore, the correlation between the two properties changes over time under physiological conditions.

3.4 Materials and Methods

Experimental design

The sample size was not determined prior to experimentations. Pixels with an outlier value were excluded when calculating the average during image processing.

The number and composition of experiments are noted in figure legends. All data were statically evaluated by comparing with control conditions or random shuffled-datasets. Alternatively, when there was no control group, datasets were compared by suitable statistic tests (Refer to “*Statistical analysis*”).

Plasmid

The mitAT1.03 plasmid (Imamura et al., 2009; Kioka et al., 2014; Yoshida et al., 2017) was kindly provided by Dr. Imamura (Kyoto University, Kyoto, Japan).

Cell culture

Dorsal root ganglion neurons dissected from Wister rat embryos at embryonic day 18 were dissociated with 1 mg/mL trypsin (Sigma-Aldrich) in phosphate-buffered saline. The dissociated cells were cultured in Neurobasal medium without phenol red (Life Technologies), supplemented with 2% B27 (Life Technologies) and 50 ng/mL nerve growth factor (NGF; Alomone Labs). Cells were transfected with mitAT1.03 by electroporation and seeded on 35-mm glass-based dishes (IWAKI) double-coated with 0.01 mg/mL poly-D-lysine (SIGMA) and 10 mg/mL laminin (Invitrogen), and cultured at 37 °C in 5% CO₂. Neurons transfected with mitAT1.03, an ATP_{mito} indicator, were also stained with tetramethylrhodamine ethyl ester (TMRE; Invitrogen), an IMP_{mito} indicator, and observed by confocal microscope 6–24 h after dissociation, coinciding with a period of axonal elongation (Fig. 3-1).

All animal procedures were approved by the Ethics Committee of Keio University (permit number, 09106-(1)). In addition, all experiments were performed in accordance with relevant guidelines and regulations.

Measurement of ATP_{mito} using mitAT1.03

Neurons were transfected with mitAT1.03 by electroporation using Neon (Life Technologies) just before plating. mitAT1.03 is a fluorescence resonance energy transfer (FRET)-based indicator, and is composed of the epsilon subunit of the F_oF₁-ATP synthase sandwiched by the cyan- and yellow-fluorescent proteins. Additionally, this indicator accompanies the duplex of the mitochondrial targeting signal of cytochrome c oxidase subunit VIII, which is a protein that is normally localized to the mitochondrial inner-membrane (Imamura et al., 2009). FRET refers to a phenomenon between donor and acceptor molecules in which the energy from the excited donor is transferred to the acceptor when the emission spectrum of a donor overlaps the absorption spectrum of an acceptor. This phenomenon occurs when the two molecules are in close proximity, although the extent of the spectral overlap and orientation between the donor and the acceptor also affect FRET efficiency. The epsilon subunit assumes its folded form upon ATP binding, and is relaxed in the absence of ATP. As a result, changes in ATP levels can be estimated from the changes in FRET signal intensity, which is derived from alternation of the relative distance and orientation between the two fluorophores.

Measurement of IMP_{mito} using TMRE

Neurons were stained 6–24 h after transfection with 25 nM TMRE for 10 min at 37°C and imaged. TMRE was not removed after the initial staining; therefore, there was additional TMRE dye at 5 nM concentration in the cytoplasm and medium during observation. TMRE is a cell-permeant and positively-charged dye, which accumulates in the relatively negatively-charged mitochondria. Because the extent of TMRE incorporation depends on the extent of mitochondrial polarization, mitochondrial polarization could be estimated from TMRE fluorescence; higher TMRE intensity indicates a greater extent of IMP_{mito} polarization (hyperpolarization).

Fluorescence microscopy

All fluorescent imaging experiments were performed using a confocal laser-scanning microscope (FV1000 IX81; OLYMPUS) with a $\times 60$ oil immersion objective lens.

mitAT1.03 and TMRE were excited by a diode laser (440 nm) and a helium-neon laser (559 nm), respectively, through a 20/80 beam splitter. Emitted fluorescence was separated by dichroic mirrors (510 nm and 560 nm), and signals from mseCFP, mVenus and TMRE were detected at 460–500 nm, 510–530 nm and 575–675 nm, respectively, using band pass filters. The widths of the 460–500 nm and 510–530 nm filters were manually adjusted using monochromators to ensure the lowest amount of background and fluorescence leakage from other channels or excitation lights (Chalmers and McCarron, 2008; Imamura et al., 2009; Yamanaka et al., 2015). Width of 575–675 nm was a specified value of a barrier filter in our system (Figs. 3-15, 3-16).

Images were acquired at regions approximately 0–150 μm from the edge of axons, with a resolution of 0.132 $\mu\text{m}/\text{pixel}$ every 10 sec for 10–15 min. During imaging, cells were maintained at 37 °C and in a 5% CO₂ atmosphere using a stage chamber (TOKAI HIT).

Correlation analysis between membrane potential and ATP of mitochondria and axonal elongation

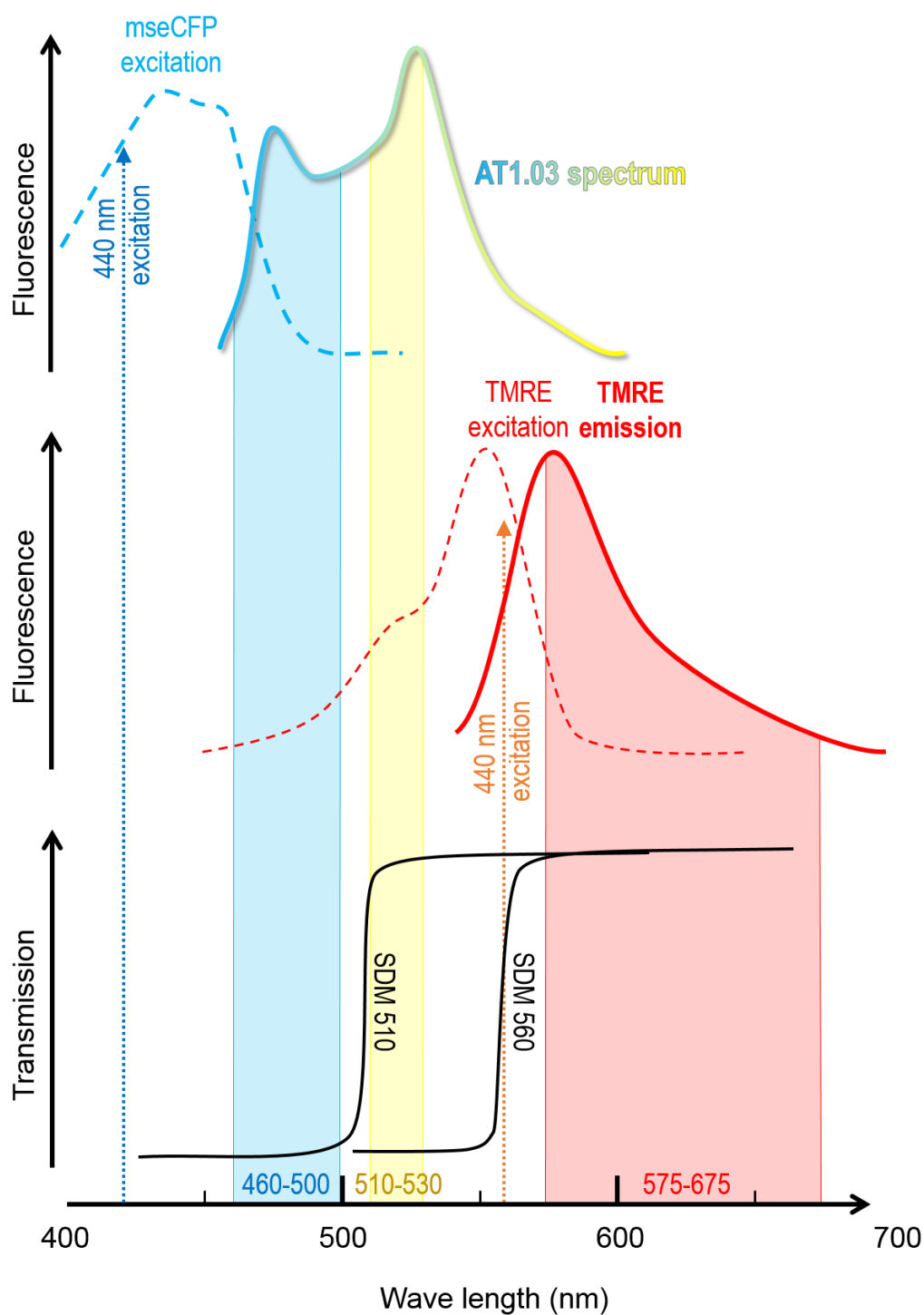


Figure 3-15. Schematic representation of the fluorescence character of probes and appropriate optical setups.

SDM is an abbreviation for signal dichroic mirror (refer to Fig. 3-16). Source: Imamura et al., 2009; Yamanaka et al., 2015; Chalmers and McCarron, 2008.

Correlation analysis between membrane potential and ATP of mitochondria and axonal elongation

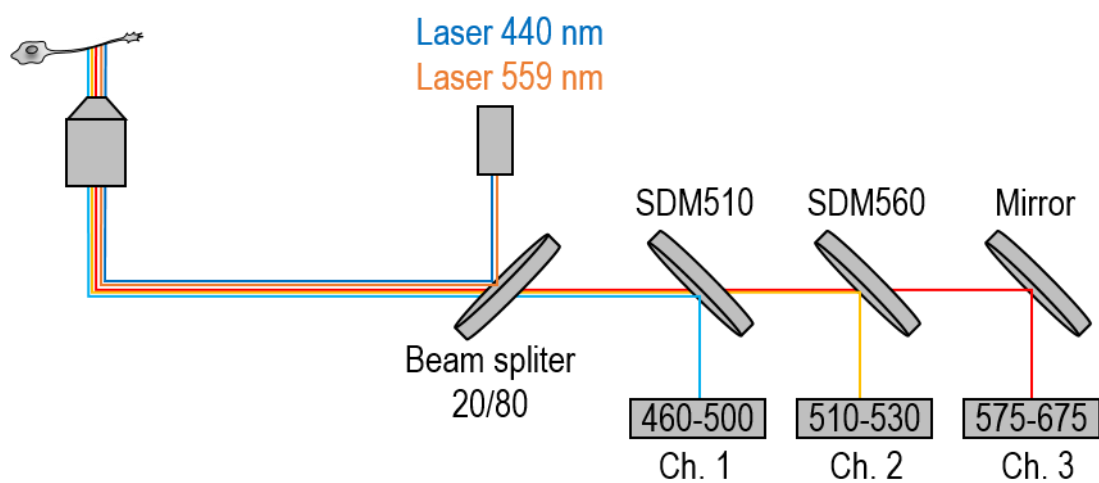


Figure 3-16. Schematic representations of microscope setup.

SDM is an abbreviation for signal dichroic mirror. 460–500, 510–530 and 575–675 represent the wavelength (in nm) of band pass filters.

Correlation analysis between membrane potential and ATP of mitochondria and axonal elongation

Image processing and analysis of mitochondrial behavior (Figs. 3-17, 3-18)

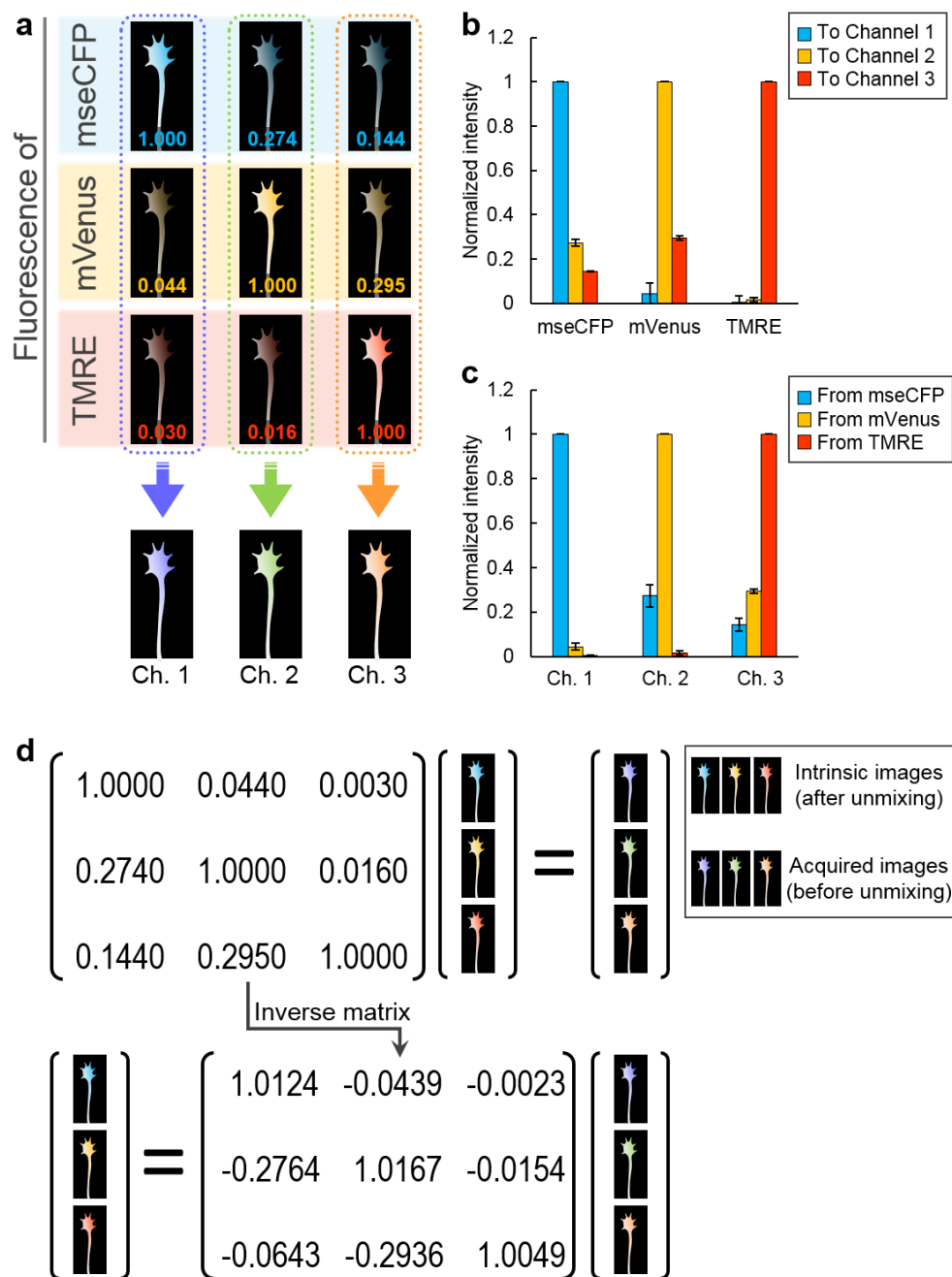
Acquired images were processed using our novel image processing software. It was written in MATLAB, and developed for this study referring to previous researches (Kobayashi et al., 2013; Suzuki et al., 2015).

Acquired fluorescent images were median filtered (3×3) and the background was subtracted. The background-subtracted images were again median filtered (3×3).

Next, to obtain signals from each fluorescent proteins or dye, linear-unmixing processing was conducted for each pixel (refer to Fig. 3-17 and the following paragraph titled “*Unmixing processing*” for detail procedure).

After linear-unmixing, images were again median filtered (3×3). Then, merged images of mseCFP and mVenus from mitAT1.03 were aligned in order of time to obtain a kymograph. A kymograph based on TMRE fluorescence was also produced. Each mitochondrial track was manually identified while referring to the both kymographs. This double check enhanced the certainness of mitochondrial detection. Position, moving direction, displacement and velocities of each mitochondrion for each time point was calculated based on the tracks. When calculating mitochondrial displacement and velocity, axonal elongation was considered. The curve of the axonal process was also corrected for the estimation of displacement and velocity. The time course of each IMP_{mito} and ATP_{mito} was estimated from averaged TMRE intensities or from the pixel-by-pixel value of mVenus/mseCFP of mitAT1.03 within a mitochondrion, respectively.

Correlation analysis between membrane potential and ATP of mitochondria and axonal elongation

**Figure 3-17. Unmixing processing procedure.**

(a) Schematic image of fluorescent leakage. Values attached to each image represent the relative intensity in each channel. (b) Fluorescent leakage into each channel. (c) Fluorescent components in each channel. (d) Schematic representation of the procedure for unmixing calculation. Error bars represent standard deviation.

Correlation analysis between membrane potential and ATP of mitochondria and axonal elongation

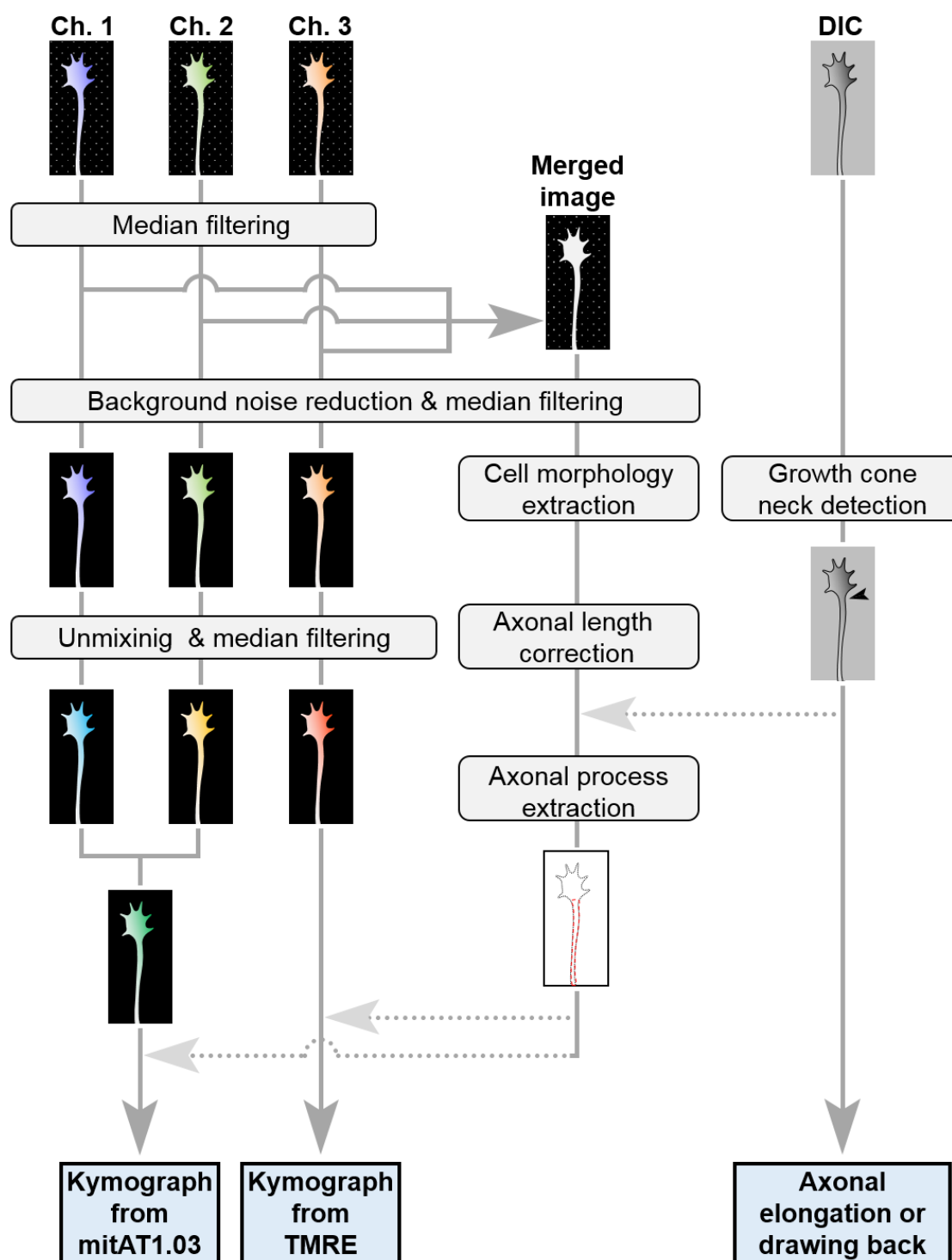


Figure 3-18. Procedure of image processing.

Overview of our image processing software. Refer to Figs. 3-15, 3-16, and 3-17 for detail of fluorescent imaging and unmixing.

Correlation analysis between membrane potential and ATP of mitochondria and axonal elongation

Unmixing processing

Cells labelled with cytosolic CFP, cytosolic Venus or TMRE were prepared and excited under experimental filter, laser and detection wavelength conditions. The acquired images were processed with background noise reduction and median filtration. Then, the cellular (for CFP- or Venus-expressing cells) or mitochondrial area (for TMRE-labelled cells) was automatically detected in each channel (Ch. 1, CFP-expressing cells; Ch. 2, Venus-expressing cells; Ch. 3, TMRE-stained cells). Relative leakage matrix was derived by quantifying the average fluorescence from the detected areas in each channel. Finally, intrinsic signals were obtained by multiplying the inverse matrix of the leakage matrix to the acquired signals pixel-by-pixel.

Image processing and analysis of neuronal behavior

Axonal elongation and drawing back after Oligomycin A or FCCP treatment were estimated by identifying neck position of the GC as a landmark in DIC images.

The neck position is a boundary point between GC and the axonal process. Because the width of the axonal process is mostly constant, the point where the width increases compared to the adjacent point was determined as the neck position. The GC neck position was visually detected in every third image, and automatically complemented for the remaining images. Axonal elongation and drawing back distances were quantified from the displacement of two neck positions. The distance of axonal elongation is a displacement of the neck positions for 10 min observation. The distance of drawing back was defined as the distance over which the GC neck position moved back at 10 minutes after drug treatment.

The software used to analyze the DIC images was originally developed for this study; however, the main procedure that utilized the manually-detected neck position as a landmark of axonal elongation was based on a previously published protocol (Kobayashi et al., 2013).

Distinguishing transport categories

The novel software used to generate kymographs was developed for the purposes of this study (Fig. 3-18).

Mitochondria with an average velocity larger than $|\pm 0.5 \times 10^{-2}| \mu\text{m}/\text{sec}$ were classified as moving mitochondria. However, some mitochondria showed not only a move status but also a pause status during the observation; mitochondria displaced more than $|\pm 1| \mu\text{m}$ were also considered as moving mitochondria. Mitochondria other than moving mitochondria were classified as stationary mitochondria. Anterograde or retrograde transport was classified based on the direction of movement. Here, velocity of a mitochondrion was estimated as (displacement distance from first position to final position during an observation [μm]) / (time of the observation [sec]), even mitochondria showed bidirectional movements. Therefore, the velocity of a mitochondrion that stopped during movement or moved bidirectionally was calculated to be slower. Other parameters such as ATP_{mito} or IMP_{mito} of a mitochondrion were calculated by averaging all time frames of which the mitochondrion was detected. For this reason, mitochondria moving across each other during the observation were excluded when deriving Figs. 3-2, 3-3, 3-4 and 3-13.

Analysis of fusion and fission events

Fusion or fission events were manually identified by referring to the corresponding kymographs and movies; kymographs provide information related to mitochondrial dynamics or the time course of ATP_{mito} or IMP_{mito} , and movies enable us to differentiate between a fusion/fission event and the overlapping/separation of two mitochondrial moving across each other. Events found in the kymograph that could not be confirmed as fission/fusion using the corresponding movies were excluded from the analysis in Fig. 3-5. During fusion events, the average IMP_{mito} or ATP_{mito} levels of two pre-fusion mitochondria were compared with those of a post-fusion mitochondrion. During fission events, the IMP_{mito} or ATP_{mito} levels of two post-fission mitochondria were compared with those of a pre-fission mitochondrion.

Correlation analysis between membrane potential and ATP of mitochondria and axonal elongation

Visualizing the correlation between ATP_{mito} levels and IMP_{mito}

We applied moving averages (1.5 min before and after) to the relative ATP_{mito} and IMP_{mito}, and demonstrated the time transition of the values using pseudo color.

Correlation analysis and random shuffling

The cross-correlation function was calculated using a MATLAB function after smoothing and normalizing the original sequential data. As a control, random-shuffled datasets were generated from the original datasets (order of each value was shuffled) and the correlation between the two control datasets was calculated.

Comparison of mitochondrial properties in the GC and axonal process

Mitochondrial density, IMP_{mito} and ATP_{mito} of Fig. 3-7 were derived from a single image that correspond to the first image of a time-lapse observation. Additionally, the morphology of the axonal process was detected using the first DIC image. Distances of axonal elongation were calculated by comparing the first and the last DIC image. Density was calculated as a ratio: (sum of area dominated by all mitochondria) / (area size of GC or axonal process). ATP_{mito} and IMP_{mito} were calculated from the average of all mitochondria included in the area of interest. The integrated ATP_{mito} signal was estimated as: (density) × (ATP_{mito}). The widths of axonal process regions (20 μm) were decided so as to have the same area as that of GCs.

Inhibitor experiments

FCCP (final concentration, 5 μM; SIGMA) or Oligomycin A (final concentration, 2 μM; SIGMA) were applied onto a glass-based dish at 5 min of the whole 15 minute observation. To evaluate changes in ATP_{mito} or IMP_{mito} after application of FCCP or Oligomycin A, the average values before and after application were compared. In Fig. 3-8c, the drawing back distance of neck positions after drug treatment was compared with the displacement of the neck positions of control neurons for 10 min under physiological conditions.

Quantification of morphological change in growth cone

In Figs. 3-9 and 3-10, morphology of growth cone was quantified by semi-automatic analysis generated by our own for this study. Briefly, growth cone morphology of every single image was manually detected for all time frames. In addition, morphology of C-domain and GC neck position were defined by manually for all these images. P-domain was defined by subtracting C-domain area from GC area. From these morphologies, area and edge length were calculated for both P-domain and C-domain, respectively. Newly appeared area and newly disappeared area were quantified by comparing the two sequential images.

Imaging of cytosolic ATP level

In Fig. 3-11, neurons expressing cytosolic ATP sensor AT1.03 (Imamura et al., 2009) were imaged. The AT1.03 plasmid was also provided by Dr. Imamura (Kyoto University, Kyoto, Japan). Cytosolic ATP levels were estimated by calculating mVenus/mseCFP ratio. GC morphology was defined from fluorescence of mseCFP + mVenus automatically. Procedures of these image processing were based on a previous study (Kobayashi et al., 2013). Latrunculin A (TOCRIS) was applied at the final concentration of 100 nM.

Statistical analysis

Data were evaluated using the Mann-Whitney U-test or Wilcoxon signed-rank test. When more than three groups were compared, Bonferroni correction was performed. As for Fig. 3e–m, Spearman's rank correlation coefficient was used. Asterisks (***, **, *) indicate a significance of < 0.001 , < 0.01 and < 0.05 , respectively.

4. Chapter 4

Conclusion

4.1 Summary

It is essential to understand local ATP dynamics under physiological conditions. However, most previous studies have focused on ATP changes resulting from non-physiological extensive stimuli, and analyses were conducted without paying attention to spatial differences inside the cell (Connolly et al., 2014; Dalton et al., 2014; Nakano et al., 2011; Surin et al., 2012; Tanaka et al., 2014). In this study, I monitored physiological and local ATP dynamics using the genetically encoded ATP sensor (Imamura et al., 2009; Yoshida et al., 2017), and evaluated the relevance of ATP to cellular morphological change using image-processing and correlation analysis.

In Chapter 2, local ATP change in the edges of HeLa cells was explored (Figs. 4-1, 4-2). The edges of these cells have two layers: the microtubule-rich inner “lamella” and the actin-rich outer “peripheral structure”. Under physiological conditions, a microtubule rush induced changes in lamella morphology, and it accompanied an increase in ATP within the lamella. The change over time in lamella ATP levels and the morphology of the peripheral structure revealed a complicated relationship under physiological conditions, and inhibitors of microtubule dynamics, actin dynamics, or ATP production each changed this complicated pattern in their own way. Microtubule inhibition reduced the extent of ATP fluctuation and the length of protrusions. Inhibition of actin also resulted in less dynamic morphological change in the peripheral structure, and caused ATP levels to remain high. Inhibition of ATP production also reduced the protrusion dynamics, and lowered ATP levels. The fact that inhibition of ATP resulted in reduced ATP levels within the cell and also suppressed change in peripheral structure morphology further supports the relevance of ATP to morphological change. The microtubule stabilizer and actin polymerization inhibitor both caused changes in lamella ATP dynamics and in the extent of morphological

change in the peripheral structure. However, the way each type of cytoskeleton participates in these ATP–morphology dynamics is likely to be different, because these two chemicals each had different effects on the pattern observed.

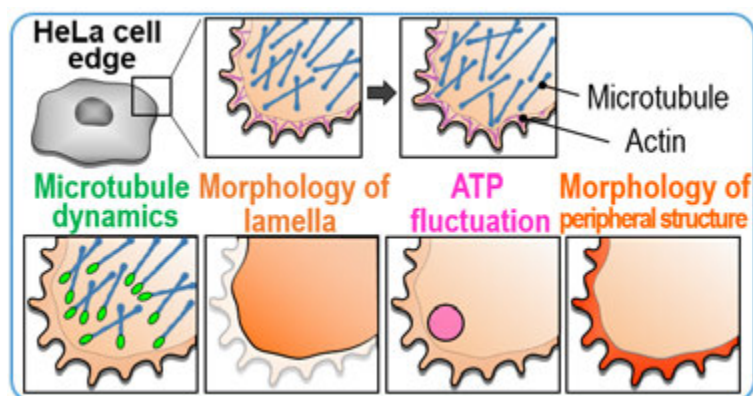


Figure 4-1. Experimental overview of Chapter 2.

Local ATP change at the edge of HeLa cells was explored. The edges of HeLa cells have two layers: microtubule-rich inner “lamella” and actin-rich outer “peripheral structure”. Correlations between microtubule dynamics, lamella area morphological change, ATP fluctuation in lamella, peripheral structure morphological change were explored.

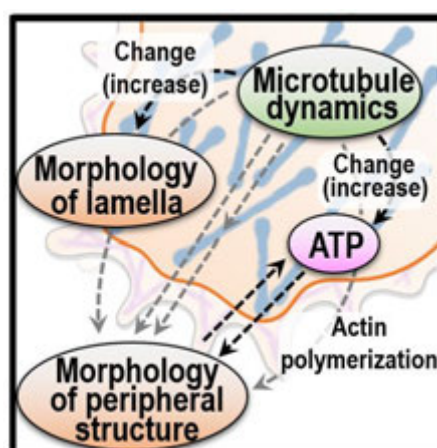


Figure 4-2. Summary of Chapter 2.

A microtubule rush affects lamella morphology, accompanied by an increase in ATP. This fluctuation in ATP is thought to be related to morphological changes in the peripheral structure, *via* actin polymerization. However, microtubule dynamics are also related to these changes in the peripheral structure, either directly or indirectly.

In Chapter 3, mitochondrial activity was evaluated in terms of inner-membrane potential (IMP_{mito}) and mitochondrial ATP (ATP_{mito}), and the relationship between this activity and axonal elongation was explored (Figs. 4-3, 4-4). Mitochondria located in axonal processes and in growth cones exhibited different activity. ATP_{mito} levels were positively correlated with axonal elongation, and this correlation was stronger in growth cone mitochondria than in the axonal processes mitochondria. In addition, IMP_{mito} exhibited no correlation with axonal elongation in either location. Furthermore, disturbance of ATP_{mito} production resulted in axonal drawing back and the collapse of growth cones. The extent of this process was correlated with the reduction in ATP_{mito} levels, but there was no correlation between IMP_{mito} and axonal drawing back. Again, the correlation was more apparent in growth cones than in axonal processes. Although it has been assumed that there is a strong correlation between IMP_{mito} and ATP_{mito} , my research has directly demonstrated for the first time that these are not always strongly correlated. Also, with respect to axonal elongation, ATP_{mito} was shown to be more important than IMP_{mito} .

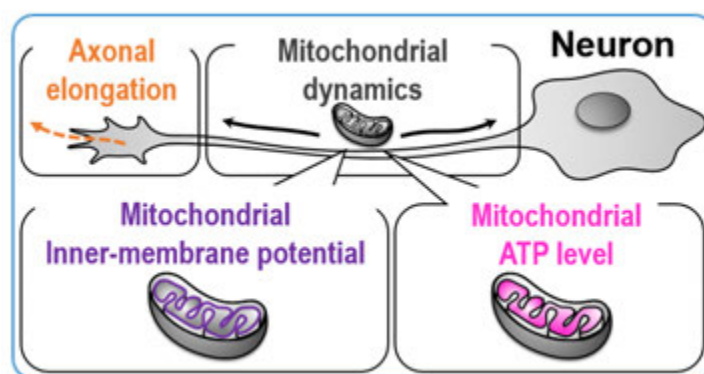


Figure 4-3. Experimental overview of Chapter 3.

Activities of mitochondria moving within neurons was evaluated in terms of inner-membrane potential and mitochondrial ATP, and explored how they relate to axonal elongation.

4.2 Significance

This study examined examples of local ATP dynamics in cells under physiological conditions. This is significant, given that only a few studies thus far have investigated local ATP dynamics, especially under physiological conditions. I succeeded in demonstrating not only local ATP dynamics, but also their relevance to morphological change. The cells I focused on were HeLa cells (their edges, in particular) and elongating neurons. Their common feature was dynamic morphological change based on active actin turnover (Sheng and Cai, 2012). The common feature of these two cell types may be one reason why I was able to visualize these phenomena despite few precedents. However, the most important reason for my success appears to have been the approach I took: a combination of simultaneous imaging and image-processing analysis. It has been several years since the live-cell ATP-imaging technique (genetically encoded ATP sensors) was developed (Imamura et al., 2009). Although this new indicator facilitates high-resolution spatiotemporal monitoring of ATP in live cells (Connolly et al., 2014; Imamura et al., 2009; Nakano et al., 2011; Surin et al., 2012; Tanaka et al., 2014), local ATP dynamics within cells or ATP behavior under physiological conditions have not yet been revealed. This is understandable because it is easier to analyze whole-cell ATP content (without considering the possibility that local differences exist within the cell), in terms of change in response to extensive stimuli (even though these stimuli lie outside the physiological range). In contrast, exploring a local area whose morphology changes dynamically requires image processing. In addition, detecting small signal changes occurring under physiological conditions also requires careful quantitative image processing. Moreover, simultaneous imaging of living cells is necessary to directly reveal the relationship between biological parameters. Thus, what this thesis shows is the usefulness of the combination of careful simultaneous imaging and detailed image-processing analysis.

Currently, new indicators are continuously being reported (Corrêa, 2014; Tamura and Hamachi, 2014), and the need to understand biological phenomena occurring under physiological conditions has increased rapidly. This study provides a successful

example of the combination of recent bioinformatics techniques, and facilitates future research into the native dynamics of biological signals.

4.3 Features and advantages of this approach

In this section, I analyze the features and advantages of the approach used in this study from three perspectives.

Analysis without artificial intervention

One of the conventional approaches to investigating relationships between two targets is to disturb one of them artificially and monitor the effect on the other. This method is effective; however, there is a risk that a relationship revealed in this way is far from the reality under physiological conditions. This is especially crucial if one or both of the targets are related to variety of cellular phenomena, because artificial interruption causes drastic changes in cellular functions under such circumstances. However, the approach described in this thesis does not require artificial interference to detect correlations. It can therefore be used to explore more-native correlations, even when the targets are engaged in a range of cellular phenomena, as is the case for ATP.

Analysis without extreme conditions

Another approach frequently used is the comparison of physiological conditions with extreme conditions. This is useful for clarifying the difference between these two states; however, comparisons with extreme conditions risk missing variation that exists within the range of physiological conditions, such as the variety of the correlations shown in Fig. 2-7 or Fig. 3-12. Since this new approach does not necessarily require comparison between conditions, it is suitable for exploring conditions that vary naturally, such as physiological conditions.

Analysis without prior identification of analytical targets

This approach uses an exploratory rather than a target-based approach to identifying correlations. It can be used to perform correlation evaluation repeatedly by testing several parameters, including temporal and spatial changes. This is useful when target selection is difficult because of a dearth of precedents, as is the case when investigating physiological and local ATP behavior.

4.4 Potential applications of this approach

In this section, I discuss two potential applications of my approach.

Combination with signal transduction analysis

Analysis of signal transduction pathways requires careful sequential evaluation of the relationships between the elements included in the pathway (Landry et al., 2015).

However, cells in real environments contain enormous numbers of such elements.

Therefore, using this approach to extract potentially relevant elements from a large pool of possibilities would enhance the efficiency of signal transduction analysis.

Combination with system perturbation

Although this approach does not require artificial interruption, it also does not preclude it; rather, combination of an artificial perturbation with this approach would be effective. As shown in Fig. 2-7, my approach enabled us to visualize not only physiological conditions, but also transition processes from a physiological condition to an abnormal condition. Exploring what is changing or how it is changing during cellular degeneration would be useful, especially for cellular processes related to disease, such as neurodegenerative processes (Dubey et al., 2015; Lin and Beal, 2006) or the transformation of normal cells to malignant tumor cells (Ward and Thompson, 2012).

References

- Ahn, B. H., Kim, H. S., Song, S., Lee, I. H., Liu, J., Vassilopoulos, A., Deng, C. X. and Finkel, T.** (2008). A role for the mitochondrial deacetylase Sirt3 in regulating energy homeostasis. *Proc. Natl. Acad. Sci. U. S. A.* **105**, 14447–14452.
- Ainscow, E. K. and Rutter, G. A.** (2002). Glucose-stimulated oscillations in free cytosolic ATP concentration imaged in single islet β -cells. *Diabetes* **51**, S162–S170.
- Ataullakhanov, F. I. and Vitvitsky, V. M.** (2002). What determines the intracellular ATP concentration. *Biosci. Rep.* **22**, 501–511.
- Attwell, D. and Laughlin, S. B.** (2001). An energy budget for signaling in the grey matter of the brain. *J. Cereb. Blood Flow Metab.* **21**, 1133–1145.
- Bernstein, B. W. and Bamburg, J. R.** (2003). Actin-ATP hydrolysis is a major energy drain for neurons. *J. Neurosci.* **23**, 1–6.
- Buccione, R., Orth, J. D. and McNiven, M. A.** (2004). Foot and mouth: podosomes, invadopodia and circular dorsal ruffles. *Nat. Rev. Mol. Cell Biol.* **5**, 647–657.
- Cain, D. F. and Davies, R. E.** (1962). Breakdown of adenosine triphosphate during a single contraction of working muscle. *Biochem. Biophys. Res. Commun.* **8**, 361–366.
- Caino, M. C., Ghosh, J. C., Chae, Y. C., Vaira, V., Rivadeneira, D. B., Favarsani, A., Rampini, P., Kossenkov, A. V., Aird, K. M., Zhang, R., et al.** (2015). PI3K therapy reprograms mitochondrial trafficking to fuel tumor cell invasion. *Proc. Natl. Acad. Sci. U. S. A.* **112**, 8638–8643.
- Chada, S. R. and Hollenbeck, P. J.** (2003). Mitochondrial movement and positioning in axons: the role of growth factor signaling. *J. Exp. Biol.* **206**, 1985–1992.
- Chada, S. R. and Hollenbeck, P. J.** (2004). Nerve growth factor signaling regulates motility and docking of axonal mitochondria. *Curr. Biol.* **14**, 1272–1276.
- Chalmers, S. and McCarron, J. G.** (2008). The mitochondrial membrane potential and Ca^{2+} oscillations in smooth muscle. *J. Cell Sci.* **121**, 75–85.
- Connolly, N. M. C., Düssmann, H., Anilkumar, U., Huber, H. J. and Prehn, J. H. M.** (2014). Single-cell imaging of bioenergetic responses to neuronal excitotoxicity and oxygen and glucose deprivation. *J. Neurosci.* **34**, 10192–10205.
- Corrêa, I. R.** (2014). Live-cell reporters for fluorescence imaging. *Curr. Opin. Chem. Biol.* **20**, 36–45.
- Dalton, C. M., Szabadkai, G. and Carroll, J.** (2014). Measurement of ATP in single oocytes: impact of maturation and cumulus cells on levels and consumption. *J. Cell. Physiol.* **229**, 353–361.
- Daniel, J. L., Molish, I. R., Robkin, L. and Holmsen, H.** (1986). Nucleotide exchange between cytosolic ATP and F-actin-bound ADP may be a major energy-utilizing process in unstimulated platelets. *Eur. J. Biochem.* **156**, 677–684.
- De Bock, K., Georgiadou, M., Schoors, S., Kuchnio, A., Wong, B. W., Cantelmo, A. R., Quaegebeur, A., Ghesquière, B., Cauwenberghs, S., Eelen, G., et al.** (2013). Role of PFKFB3-driven glycolysis in vessel sprouting. *Cell* **154**, 651–663.
- Downing, K. H.** (2000). Structural basis for the interaction of tubulin with proteins and drugs that affect microtubule dynamics. *Annu. Rev. Cell Dev. Biol.* **16**, 89–111.
- Dubey, J., Ratnakaran, N. and Koushika, S. P.** (2015). Neurodegeneration and microtubule dynamics: death by a thousand cuts. *Front. Cell. Neurosci.* **9**, 343.

- Fukumitsu, K., Fujishima, K., Yoshimura, A., Wu, Y. K., Heuser, J. and Kengaku, M.** (2015). Synergistic action of dendritic mitochondria and creatine kinase maintains ATP homeostasis and actin dynamics in growing neuronal dendrites. *J. Neurosci.* **35**, 5707–5723.
- Gerencser, A. A., Mookerjee, S. A., Jastroch, M. and Brand, M. D.** (2017). Positive feedback amplifies the response of mitochondrial membrane potential to glucose concentration in clonal pancreatic beta cells. *Biochim. Biophys. Acta* **1863**, 1054–1065.
- Gierke, S. and Wittmann, T.** (2012). EB1-recruited microtubule + TIP complexes coordinate protrusion dynamics during 3D epithelial remodeling. *Curr. Biol.* **22**, 753–762.
- Gledhill, J. R., Montgomery, M. G., Leslie, A. G. W. and Walker, J. E.** (2007). How the regulatory protein, IF₁, inhibits F₁-ATPase from bovine mitochondria. *Proc. Natl. Acad. Sci. U. S. A.* **104**, 15671–15676.
- Groschner, L. N., Waldeck-Weiermair, M., Malli, R. and Graier, W. F.** (2012). Endothelial mitochondria-less respiration, more integration. *Pflugers Arch Eur J Physiol* **464**, 63–76.
- Hara, K. Y. and Kondo, A.** (2015). ATP regulation in bioproduction. *Microb. Cell Fact.* **14**, 198.
- Harris, J. J., Jolivet, R. and Attwell, D.** (2012). Synaptic energy use and supply. *Neuron* **75**, 762–777.
- Hattori, T., Watanabe, K., Uechi, Y., Yoshioka, H. and Ohta, Y.** (2005). Repetitive transient depolarizations of the inner mitochondrial membrane induced by proton pumping. *Biophys. J.* **88**, 2340–2349.
- Haworth, R. A. and Hunter, D. R.** (1979). The Ca²⁺-induced membrane transition in mitochondria. *Arch. Biochem. Biophys.* **195**, 460–467.
- Hayashi, K., Suzuki, A., Hirai, S., Kurihara, Y., Hoogenraad, C. C. and Ohno, S.** (2011). Maintenance of dendritic spine morphology by partitioning-defective 1b through regulation of microtubule growth. *J. Neurosci.* **31**, 12094–12103.
- Imamura, H., Huynh Nhat, K. P., Togawa, H., Saito, K., Iino, R. and Kato-Yamada, Y.** (2009). Visualization of ATP levels inside single living cells with fluorescence resonance energy transfer-based genetically encoded indicators. *Proc. Natl. Acad. Sci. U. S. A.* **106**, 15651–15656.
- Jaworski, J., Kapitein, L. C., Gouveia, S. M., Dortland, B. R., Wulf, P. S., Grigoriev, I., Camera, P., Spangler, S. A., Di Stefano, P., Demmers, J., et al.** (2009). Dynamic microtubules regulate dendritic spine morphology and synaptic plasticity. *Neuron* **61**, 85–100.
- Kennedy, H. J., Pouli, A. E., Ainscow, E. K., Jouaville, L. S., Rizzuto, R. and Rutter, G. A.** (1999). Glucose generates sub-plasma membrane ATP microdomains in single islet β -cells: potential role for strategically located mitochondria. *J. Biol. Chem.* **274**, 13281–13291.
- Kioka, H., Kato, H., Fujikawa, M., Tsukamoto, O., Suzuki, T., Imamura, H., Nakano, A., Higo, S., Yamazaki, S., Matsuzaki, T., et al.** (2014). Evaluation of intramitochondrial ATP levels identifies G0/G1 switch gene 2 as a positive regulator of oxidative phosphorylation. *Proc. Natl. Acad. Sci. U. S. A.* **111**, 273–278.
- Klotzsch, E., Smorodchenko, A., Löfler, L., Moldzio, R., Parkinson, E., Schütz, G. J. and Pohl, E. E.** (2015). Superresolution microscopy reveals spatial separation of UCP4 and F₀F₁-ATP synthase in neuronal mitochondria. *Proc. Natl. Acad. Sci. U. S. A.* **112**, 130–135.
- Kobayashi, T., Nagase, F., Hotta, K. and Oka, K.** (2013). Crosstalk between second messengers predicts the motility of the growth cone. *Sci. Rep.* **3**, 3118.
- Kruchten, A. E. and McNiven, M. A.** (2006). Dynamins as a mover and pincher during cell migration and invasion. *J. Cell Sci.* **119**, 1683–1690.
- Ladoux, B. and Nicolas, A.** (2012). Physically based principles of cell adhesion mechanosensitivity in tissues. *Rep. Prog. Phys.* **75**, 116601.
- Lamprecht, R. and LeDoux, J.** (2004). Structural plasticity and memory. *Nat. Rev. Neurosci.* **5**, 45–54.

- Landry, B. D., Clarke, D. C. and Lee, M. J.** (2015). Studying cellular signal transduction with OMIC technologies. *J. Mol. Biol.* **427**, 3416–3440.
- Lin, M. T. and Beal, M. F.** (2006). Mitochondrial dysfunction and oxidative stress in neurodegenerative diseases. *Nature* **443**, 787–795.
- Lukic-Bilela, L., Perovic-Ottstadt, S., Walenta, S., Natalio, F., Plese, B., Link, T. and Müller, W. E. G.** (2011). ATP distribution and localization of mitochondria in *Suberites domuncula* (Olivi 1792) tissue. *J. Exp. Biol.* **214**, 1748–1753.
- MacAskill, A. F. and Kittler, J. T.** (2010). Control of mitochondrial transport and localization in neurons. *Trends Cell Biol.* **20**, 102–112.
- Machacek, M. and Danuser, G.** (2006). Morphodynamic profiling of protrusion phenotypes. *Biophys. J.* **90**, 1439–1452.
- Massé, K., Bhamra, S., Eason, R., Dale, N. and Jones, E. A.** (2007). Purine-mediated signalling triggers eye development. *Nature* **449**, 1058–1062.
- Matov, A., Applegate, K., Kumar, P., Thoma, C., Krek, W., Danuser, G. and Wittmann, T.** (2010). Analysis of microtubule dynamic instability using a plus-end growth marker. *Nat. Methods* **7**, 761–768.
- McLaughlin, A. C., Takeda, H. and Chance, B.** (1979). Rapid ATP assays in perfused mouse liver by ³¹P NMR. *Proc. Natl. Acad. Sci. U. S. A.* **76**, 5445–5449.
- Miller, K. E. and Sheetz, M. P.** (2004). Axonal mitochondrial transport and potential are correlated. *J. Cell Sci.* **117**, 2791–2804.
- Morrison, E. E., Moncur, P. M. and Askham, J. M.** (2002). EB1 identifies sites of microtubule polymerisation during neurite development. *Mol. Brain Res.* **98**, 145–152.
- Morton, W. M., Ayscough, K. R. and McLaughlin, P. J.** (2000). Latrunculin alters the actin-monomer subunit interface to prevent polymerization. *Nat. Cell Biol.* **2**, 376–378.
- Nakano, M., Imamura, H., Nagai, T. and Noji, H.** (2011). Ca²⁺ regulation of mitochondrial ATP synthesis visualized at the single cell level. *ACS Chem. Biol.* **6**, 709–715.
- Nedergaard, J., Ricquier, D. and Kozak, L. P.** (2005). Uncoupling proteins: current status and therapeutic prospects. *EMBO Rep.* **6**, 917–921.
- Nicholls, D. G. and Budd, S. L.** (2000). Mitochondria and neuronal survival. *Physiol. Rev.* **80**, 315–360.
- O'Reilly, C. M., Fogarty, K. E., Drummond, R. M., Tuft, R. A. and Walsh, J. V. Jr.** (2003). Quantitative analysis of spontaneous mitochondrial depolarizations. *Biophys. J.* **85**, 3350–3357.
- Oruganty-Das, A., Ng, T., Udagawa, T., Goh, E. L. K. and Richter, J. D.** (2012). Translational control of mitochondrial energy production mediates neuron morphogenesis. *Cell Metab.* **16**, 789–800.
- Plucińska, G., Paquet, D., Hruscha, A., Godinho, L., Haass, C., Schmid, B. and Misgeld, T.** (2012). *In vivo* imaging of disease-related mitochondrial dynamics in a vertebrate model system. *J. Neurosci.* **32**, 16203–16212.
- Pullman, M. E. and Monroy, G. C.** (1963). A naturally occurring inhibitor of mitochondrial adenosine triphosphatase. *J. Biol. Chem.* **238**, 3762–3769.
- Rangaraju, V., Calloway, N. and Ryan, T. A.** (2014). Activity-driven local ATP synthesis is required for synaptic function. *Cell* **156**, 825–835.
- Rardin, M. J., Newman, J. C., Held, J. M., Cusack, M. P., Sorensen, D. J., Li, B., Schilling, B., Mooney, S. D., Kahn, C. R., Verdin, E., et al.** (2013). Label-free quantitative proteomics of the lysine acetylome in mitochondria identifies substrates of SIRT3 in metabolic pathways. *Proc. Natl. Acad. Sci. U. S. A.* **110**, 6601–6606.
- Rolfe, D. F. S. and Brown, G. C.** (1997). Cellular energy utilization and molecular origin of standard metabolic rate in mammals. *Physiol. Rev.* **77**, 731–758.

- Rostovtseva, T. and Colombini, M.** (1997). VDAC channels mediate and gate the flow of ATP: implications for the regulation of mitochondrial function. *Biophys. J.* **72**, 1954–1962.
- Saxton, W. M. and Hollenbeck, P. J.** (2012). The axonal transport of mitochondria. *J. Cell Sci.* **125**, 2095–2104.
- Sheng, Z. H.** (2014). Mitochondrial trafficking and anchoring in neurons: new insight and implications. *J. Cell Biol.* **204**, 1087–1098.
- Sheng, Z. H. and Cai, Q.** (2012). Mitochondrial transport in neurons: impact on synaptic homeostasis and neurodegeneration. *Nat. Rev. Neurosci.* **13**, 77–93.
- Shibata, T., Yamashita, S., Hirusaki, K., Katoh, K. and Ohta, Y.** (2015). Isolation of mitochondria by gentle cell membrane disruption, and their subsequent characterization. *Biochem. Biophys. Res. Commun.* **463**, 563–568.
- Smith, J. B., Sternweis, P. C. and Heppel, L. A.** (1975). Partial purification of active delta and epsilon subunits of the membrane ATPase from *Escherichia coli*. *J. Supramol. Struct.* **3**, 248–255.
- Spector, I., Braet, F., Shochet, N. R. and Bubb, M. R.** (1999). New anti-actin drugs in the study of the organization and function of the actin cytoskeleton. *Microsc. Res. Tech.* **47**, 18–37.
- Spillane, M., Ketschek, A., Merianda, T. T., Twiss, J. L. and Gallo, G.** (2013). Mitochondria coordinate sites of axon branching through localized intra-axonal protein synthesis. *Cell Rep.* **5**, 1564–1575.
- Srinivasan, B.** (2015). Mitochondrial permeability transition pore : an enigmatic gatekeeper. *New Horizons Sci. Technol.* **1**, 47–51.
- Stepanova, T., Slemmer, J., Hoogenraad, C. C., Lansbergen, G., Dortland, B., De Zeeuw, C. I., Grosveld, F., van Cappellen, G., Akhmanova, A. and Galjart, N.** (2003). Visualization of microtubule growth in cultured neurons via the use of EB3-GFP (End-Binding Protein 3-Green Fluorescent Protein). *J. Neurosci.* **23**, 2655–2664.
- Strehler, B. L. and McElroy, W. D.** (1957). Assay of adenosine triphosphate. *Methods Enzymol.* **3**, 871–873.
- Surin, A. M., Khiroug, S., Gorbacheva, L. R., Khodorov, B. I., Pinelis, V. G. and Khiroug, L.** (2013). Comparative analysis of cytosolic and mitochondrial ATP synthesis in embryonic and postnatal hippocampal neuronal cultures. *Front. Mol. Neurosci.* **5**, 102.
- Suzuki, R., Hotta, K. and Oka, K.** (2015). Spatiotemporal quantification of subcellular ATP levels in a single HeLa cell during changes in morphology. *Sci. Rep.* **5**, 16874.
- Swiech, L., Blazejczyk, M., Urbanska, M., Pietruszka, P., Dortland, B. R., Malik, A. R., Wulf, P. S., Hoogenraad, C. C. and Jaworski, J.** (2011). CLIP-170 and IQGAP1 cooperatively regulate dendrite morphology. *J. Neurosci.* **31**, 4555–4568.
- Takahara, Y., Inatani, M., Eto, K., Inoue, T., Kreymerman, A., Miyake, S., Ueno, S., Nagaya, M., Nakanishi, A., Iwao, K., et al.** (2015). In vivo imaging of axonal transport of mitochondria in the diseased and aged mammalian CNS. *Proc. Natl. Acad. Sci. U. S. A.* **112**, 10515–10520.
- Tamura, T. and Hamachi, I.** (2014). Recent progress in design of protein-based fluorescent biosensors and their cellular applications. *ACS Chem. Biol.* **9**, 2708–2717.
- Tanaka, T., Nagashima, K., Inagaki, N., Kioka, H., Takashima, S., Fukuoka, H., Noji, H., Kakizuka, A. and Imamura, H.** (2014). Glucose-stimulated single pancreatic islets sustain increased cytosolic ATP levels during initial Ca^{2+} influx and subsequent Ca^{2+} oscillations. *J. Biol. Chem.* **289**, 2205–2216.
- Tao, K., Matsuki, N. and Koyama, R.** (2014). AMP-activated protein kinase mediates activity-dependent axon branching by recruiting mitochondria to axon. *Dev. Neurobiol.* **74**, 557–573.
- Toloe, J., Mollajew, R., Kügler, S. and Mironov, S. L.** (2014). Metabolic differences in hippocampal 'Rett' neurons revealed by ATP imaging. *Mol. Cell. Neurosci.* **59**, 47–56.

- Tsukada, Y., Aoki, K., Nakamura, T., Sakumura, Y., Matsuda, M. and Ishii, S.** (2008). Quantification of local morphodynamics and local GTPase activity by edge evolution tracking. *PLoS Comput. Biol.* **4**, e1000223.
- Twig, G., Elorza, A., Molina, A. J. A., Mohamed, H., Wikstrom, J. D., Walzer, G., Stiles, L., Haigh, S. E., Katz, S., Las, G., et al.** (2008). Fission and selective fusion govern mitochondrial segregation and elimination by autophagy. *EMBO J.* **27**, 433–446.
- Vaarmann, A., Mandel, M., Zeb, A., Wareski, P., Liiv, J., Kuum, M., Antsov, E., Liiv, M., Cagalinec, M., Choubey, V., et al.** (2016). Mitochondrial biogenesis is required for axonal growth. *Development* **143**, 1981–1992.
- Vasilyeva, E. A., Minkov, I. B., Fitin, A. F. and Vinogradov, A. D.** (1982). Kinetic mechanism of mitochondrial adenosine triphosphatase. *Biochem. J.* **202**, 9–14.
- Verburg, J. and Hollenbeck, P. J.** (2008). Mitochondrial membrane potential in axons increases with local nerve growth factor or semaphorin signaling. *J. Neurosci.* **28**, 8306–8315.
- Wang, J., Sanger, J. M. and Sanger, J. W.** (2005). Differential effects of Latrunculin-A on myofibrils in cultures of skeletal muscle cells: insights into mechanisms of myofibrillogenesis. *Cell Motil. Cytoskeleton* **62**, 35–47.
- Wang, W., Wang, X., Fujioka, H., Hoppel, C., Whone, A. L., Caldwell, M. A., Cullen, P. J., Liu, J. and Zhu, X.** (2016). Parkinson’s disease-associated mutant VPS35 causes mitochondrial dysfunction by recycling DLP1 complexes. *Nat. Med.* **22**, 54–63.
- Ward, P. S. and Thompson, C. B.** (2012). Metabolic reprogramming: a cancer hallmark even Warburg did not anticipate. *Cancer Cell* **21**, 297–308.
- Yamanaka, M., Saito, K., Smith, N. I., Arai, Y., Uegaki, K., Yonemaru, Y., Mochizuki, K., Kawata, S., Nagai, T. and Fujita, K.** (2015). Visible-wavelength two-photon excitation microscopy for fluorescent protein imaging. *J. Biomed. Opt.* **20**, 101202.
- Yoshida, T., Alfaqaan, S., Sasaoka, N. and Imamura, H.** (2017). Application of FRET-based biosensor “ATeam” for visualization of ATP levels in the mitochondrial matrix of living mammalian cells. *Methods Mol. Biol.* **1567**, 231–243.
- Yu, Y., Lee, H. C., Chen, K. C., Suhan, J., Qiu, M., Ba, Q. and Yang, G.** (2016). Inner membrane fusion mediates spatial distribution of axonal mitochondria. *Sci. Rep.* **6**, 18981.
- Yuste, R. and Bonhoeffer, T.** (2001). Morphological changes in dendritic spines associated with long-term synaptic plasticity. *Annu. Rev. Neurosci.* **24**, 1071–1089.
- Zawistowski, J. S., Sabouri-Ghomi, M., Danuser, G., Hahn, K. M. and Hodgson, L.** (2013). A RhoC biosensor reveals differences in the activation kinetics of RhoA and RhoC in migrating cells. *PLoS One* **8**, e79877.
- Zhou, B., Lin, M. Y., Sun, T., Knight, A. L. and Sheng, Z. H.** (2014). Characterization of mitochondrial transport in neurons. *Methods Enzymol.* **547**, 75–96.

All figures included in this thesis are from open-access articles distributed under the terms of the Creative Commons Attribution License, which permits unrestricted use, distribution, and reproduction in any medium, provided the original author and source are credited.
<https://creativecommons.org/licenses/by/4.0/>

List of published papers and conference presentations

Articles on periodicals (related to this thesis)

- (1) [Rika Suzuki](#); Kohji Hotta; Kotaro Oka, Spatiotemporal quantification of subcellular ATP levels in a single HeLa cell during changes in morphology, *Scientific Reports* 5:16874, published November 17, 2015.
- (2) [Rika Suzuki](#); Kohji Hotta; Kotaro Oka, Transitional correlation between inner-membrane potential and ATP levels of neuronal mitochondria, *Scientific Reports*, in press.

Presentations at international conferences

- (1) [Rika Suzuki](#), Kohji Hotta, Kotaro Oka, Simultaneous Imaging of EB3 and ATP reveals the mechanism of cell shape control in HeLa cells, Society for Neuroscience, Washington, DC, USA, presented on November 15, 2014.
- (2) [Rika Suzuki](#), Fumiaki Nagase, Kohji Hotta, Kotaro Oka, Correlation analysis of ATP levels and morphological change during neurite extension, Society for Neuroscience, Chicago, USA, presented on October 20, 2015.
- (3) [Rika Suzuki](#), Kohji Hotta, Kotaro Oka, Spatiotemporal quantification of intracellular ATP within elongating neurites, NIG International Symposium 2016, Tokyo, Japan, presented on January 9, 2016.
- (4) [Rika Suzuki](#), Kohji Hotta, Kotaro Oka, Simultaneous imaging of ATP levels and membrane potential in mitochondria during axonal transport, Society for Neuroscience, San Diego, USA, presented on November 13, 2016.
- (5) [Rika Suzuki](#), Kohji Hotta, Kotaro Oka, Relation analysis between subcellular ATP levels and cellular morphological change, IGER International Symposium on "Now in actin study: Motor protein research reaching a new stage", Nagoya, Japan, presented on December 12, 2016.
- (6) [Rika Suzuki](#), Kohji Hotta, Kotaro Oka, Native dynamics of mitochondrial membrane potential and ATP levels in growing neurites visualized by simultaneous imaging, Society for Neuroscience, Washington, DC, USA, presented on November 12, 2017
- (7) Mitsuru Iizumi, [Rika Suzuki](#), Ryu Yamanaka, Yutaka Shindo, Kohji Hotta, Kotaro Oka, Estimation of metabolic energy balance in neurons by using fluorescent imagings, Society for Neuroscience, Washington, DC, USA, presented on November 13, 2017.

Presentations at domestic meetings

- (1) [Rika Suzuki](#), Kohji Hotta, Kotaro Oka, Cytoskeletal Dynamics Changes Intracellular ATP level, International Symposium on Multi-dimensional Fluorescence Live Imaging of Cellular Functions and Molecular Activities, Kyoto, Japan, presented on January 26, 2015.
- (2) [Rika Suzuki](#), Kohji Hotta, Kotaro Oka, Correlation of local ATP levels and morphological changes in growth cones, The 38th Annual Meeting of the Japan Neuroscience Society, Kobe, Japan, presented on July 30, 2015.
- (3) [Rika Suzuki](#), Kohji Hotta, Kotaro Oka, Simultaneous imaging and correlation analysis of mitochondrial trafficking and its ATP production, The 53th Annual Meeting of the Biophysical Society of Japan, Kanazawa, Japan, presented on September 13, 2015.
- (4) 鈴木李夏、堀田耕司、岡浩太郎、成長円錐における ATP レベル - 形態変化相関の評価、第 24 回日本バイオイメージング学会学術集会、東京、2015 年 9 月 28 日発表済

- (5) 鈴木李夏、堀田耕司、岡浩太郎、神経突起におけるミトコンドリア動態・活性の同時イメージングとその定量的評価、文部科学省 私立大学戦略的研究基盤形成支援事業ビッグデータ駆動型創薬システム研究拠点 第2回シンポジウム、横浜、2016年3月17日発表済
- (6) Rika Suzuki, Kohji Hotta, Kotaro Oka, Analysis of mitochondrial movement and its ATP production in elongating neurons, The 39th Annual Meeting of the Japan Neuroscience Society, Yokohama, Japan, presented on July 20, 2016.
- (7) 鈴木李夏、堀田耕司、岡浩太郎、伸長する神経突起でのミトコンドリア輸送・膜電位・ATP同時イメージング、第25回日本バイオイメーキング学会学術集会、名古屋、2016年9月5日発表済
- (8) Rika Suzuki, Kohji Hotta, Kotaro Oka, Correlation analysis of transport, membrane potential, and ATP levels of mitochondria and neurite extension, The 54th Annual Meeting of the Biophysical Society of Japan, Tsukuba, Japan, presented on November 26, 2016.
- (9) 鈴木李夏、堀田耕司、岡浩太郎、蛍光イメージングによる神経ミトコンドリアの膜電位・ATP同時定量、文部科学省 私立大学戦略的研究基盤形成支援事業ビッグデータ駆動型創薬システム研究拠点 第3回シンポジウム、横浜、2017年3月7日発表済
- (10) Mitsuru Iizumi, Rika Suzuki, Ryu Yamanaka, Yutaka Shindo, Kohji Hotta, Kotaro Oka, Estimation of energy metabolism by fluorescent imagings, The 40th Annual Meeting of the Japan Neuroscience Society, Chiba, Japan, presented on July 20, 2017.
- (11) Rika Suzuki, Kohji Hotta, Kotaro Oka, Simultaneous and multi-sided assessment of native mitochondrial behavior in elongating neurons, The 40th Annual Meeting of the Japan Neuroscience Society, Chiba, Japan, presented on July 21, 2017.
- (12) Rika Suzuki, Kohji Hotta, Kotaro Oka, Quantitative analysis of mitochondrial activities and its role for neurite extension, 第1回慶應ライフサイエンスシンポジウム、横浜、2017年8月28日発表済
- (13) 飯泉美弦、鈴木李夏、山中龍、新藤豊、堀田耕司、岡浩太郎、蛍光イメージング法によるエネルギー代謝評価、第1回慶應ライフサイエンスシンポジウム、横浜、2017年8月28日発表済。
- (14) Rika Suzuki, Kohji Hotta, Kotaro Oka, Simultaneous imaging of subcellular ATP dynamics and changes in cell morphology, The 26th annual meeting of the Bioimaging society, Tokyo, Japan, presented on September 17, 2017.
- (15) Rika Suzuki, Kohji Hotta, Kotaro Oka, Spatiotemporal quantification of native ATP dynamics during changes in cellular morphology, The 55th Annual Meeting of the Biophysical Society of Japan, Kumamoto, Japan, presented on September 19, 2017.

Acknowledgment

This study was conducted under the tutelage of Prof. Kotaro Oka during my doctoral course at Keio University. First of all, I must thank Prof. Oka. His sophisticated advice always helped me with my work. What I have experienced over the last five years, I owe to him and the atmosphere of freedom present in this laboratory.

I would like to thank Prof. Masaya Imoto, Prof. Nobuhide Doi, and Dr. Akira Funahashi for acting as my reviewers at the doctoral degree screening. Their comments and advice, coming from multiple points of view, provided valuable insights and helped me improve my thesis.

I am sincerely thankful to Dr. Hiromi Imamura of Kyoto University for providing a series of ATP sensors. This study would have not been possible without these sophisticated tools.

I would like to thank Dr. Kohji Hotta for his support of my research. His kind words were a continual encouragement in my daily research life.

I must express my gratitude to Dr. Yutaka Shindo. He taught me not only experimental methods but also the attitude to study. His advice, based on his rich store of experience, was of immense help in my research. I would also like to thank Dr. Ryu Yamanaka, whose teachings influenced the basis of my research greatly. I have always tried to emulate his examples in areas such as experimental techniques, image processing analysis, the design of figures, and the preparation of presentations.

I would like to thank Toshinobu Shimoi, Esq. for his advice especially on statistical analyses. I also would like to express my gratitude to Dr. Hisashi Shidara. He was the embodiment of what researchers and teachers ought to be.

I also thank the other lab members whom I could not individually mention above.

I would like to express my greatest gratitude to the Yoshida Scholarship Foundation (YSF). Their financial assistance greatly supported my study life. Moreover, the YSF family's warm and kind personalities touched my heart; supportive words from staff in the executive office and from professors encouraged me again and again. Interactions

with other Doctor 21, Master 21, and Leader 21 students always gave me power and braveness to keep holding on. I regard the relationships with YSF members as one of the great treasures in my doctoral course, and I would like to thank every single YSF member again.

I also received financial support from a number of other scholarship foundations during my studying career. I would like to thank Nakamura Sekizenkai and the Japan Student Services Organization. Moreover, I was supported by several scholarships provided by Keio University and the old boys and old girls of the university. Outside the connections regarding scholarships, I have also made the acquaintance of several respectable seniors of this university during my school days. This is one of the grateful features of Keio University. I am thankful to Keio University for providing such opportunities, and I promise to pay it forward to younger generations in the future.

I would like to thank my doctoral friends in various universities. Their presence always encouraged me. Especially, I am thankful to Yuki Kuchitsu for her understanding and warm support. In addition, I really thank Yuichiro Nakai who had studied in the same department before. His advice about my research and carriers helped me repeatedly. I also would like to express my gratitude to Dr. Luan Luu in Australia, who as a friend studying in the same field of neuroscience provided me with useful advice on my research.

I am thankful to my old schoolmates who always supported and encouraged me. Their warm congratulations for my successes remain an irreplaceable treasure in my life. I will never forget. Thank you.

I also thank all others who were not mention above yet had literally given me a hand.

I heartily thank Fumiaki Nagase, my senior colleague and a mentor of my life. My research life with him was really exciting and reassuring. He has been the best supporter I could have hoped for even after his graduation. What we spoke about together was just what I needed at that time. Thank you so much. I owe what I am today to you.

Finally, my most heartfelt thanks go to my family members for their generous supports and understanding. I was able to do my best because of your continuous help. It is thanks to you that I was able to come this far. Thank you ever so much.